The role of group IIF-secreted phospholipase A_2 in epidermal homeostasis and hyperplasia

Kei Yamamoto,[1] Yoshimi Miki,[1] Mariko Sato,[1,2] Yoshitaka Taketomi,[1] Yasumasa Nishito,[3] Choji Taya,[3] Kazuaki Muramatsu,[2] Kazutaka Ikeda,[4] Hiroki Nakanishi,[5] Ryo Taguchi,[6] Naotomo Kambe,[7] Kenji Kabashima,[8] Gérard Lambeau,[9] Michael H. Gelb,[10] and Makoto Murakami[1,11]

[1]Lipid Metabolism Project, Tokyo Metropolitan Institute of Medical Science, Tokyo 156-8506, Japan
[2]School of Science and Engineering, Tokyo Denki University, Saitama 350-0394, Japan
[3]Center for Basic Technology Research, Tokyo Metropolitan Institute of Medical Science, Tokyo 156-8506, Japan
[4]Laboratory for Metabolomics, Institute of Physical and Chemical Research (RIKEN) Center for Integrative Medical Sciences, Kanagawa 230-0045, Japan
[5]Research Center for Biosignal, Akita University, Akita 010-8543, Japan
[6]College of Bioscience and Biotechnology, Chubu University, Aichi 487-8501, Japan
[7]Department of Dermatology, Chiba University Graduate School of Medicine, Chiba 260-8677, Japan
[8]Department of Dermatology, Kyoto University Graduate School of Medicine, Kyoto 606-8507, Japan
[9]Institut de Pharmacologie Moléculaire et Cellulaire, UMR7275, Centre National de la Recherche Scientifique et Université de Nice-Sophia-Antipolis, 06560 Valbonne, France
[10]Departments of Chemistry and Biochemistry, University of Washington, Seattle, WA 98195
[11]CREST, Japan Agency for Medical Research and Development (AMED) and Japan Science and Technology Agency (JST), Tokyo 100-0004, Japan

Epidermal lipids are important for skin homeostasis. However, the entire picture of the roles of lipids, particularly nonceramide lipid species, in epidermal biology still remains obscure. Here, we report that PLA2G2F, a functionally orphan-secreted phospholipase A_2 expressed in the suprabasal epidermis, regulates skin homeostasis and hyperplasic disorders. *Pla2g2f*$^{-/-}$ mice had a fragile stratum corneum and were strikingly protected from psoriasis, contact dermatitis, and skin cancer. Conversely, *Pla2g2f*-overexpressing transgenic mice displayed psoriasis-like epidermal hyperplasia. Primary keratinocytes from *Pla2g2f*$^{-/-}$ mice showed defective differentiation and activation. PLA2G2F was induced by calcium or IL-22 in keratinocytes and preferentially hydrolyzed ethanolamine plasmalogen-bearing docosahexaenoic acid secreted from keratinocytes to give rise to unique bioactive lipids (i.e., protectin D1 and 9*S*-hydroxyoctadecadienoic acid) that were distinct from canonical arachidonate metabolites (prostaglandins and leukotrienes). Ethanolamine lysoplasmalogen, a PLA2G2F-derived marker product, rescued defective activation of *Pla2g2f*$^{-/-}$ keratinocytes both in vitro and in vivo. Our results highlight PLA2G2F as a previously unrecognized regulator of skin pathophysiology and point to this enzyme as a novel drug target for epidermal-hyperplasic diseases.

CORRESPONDENCE
Makoto Murakami:
murakami-mk@igakuken.or.jp

Abbreviations used: 10,17-diHDoHE, 10*S*, 17*S*-dihydroxy-DHA; AA, arachidonic acid; DHA, docosahexaenoic acid; DMBA, 9,10-dimethylbenz(a)anthracene; DNFB, dinitrofluorobenzene; EPA, eicosapentaenoic acid; ESI-MS, electrospray ionization mass spectrometry; HODE, hydroxyoctadecadienoic acid; IMQ, imiquimod; LA, linoleic acid; LOX, lipoxygenase; LPC, lysophosphatidylcholine; LPE, lysophosphatidylethanolamine; MRM, multiple reaction monitoring; P-LPE, plasmalogen forms of lysophosphatidylethanolamine; P-PE, plasmalogen form of phosphatidylethanolamine; PC, phosphatidylcholine; PD1, protectin D1 (10*R*, 17*S*-dihydroxy-DHA); PE, phosphatidylethanolamine; PG, prostaglandin; PLA_2, phospholipase A_2; PUFA, polyunsaturated fatty acid; RvD1, resolvin D1; SC, stratum corneum; $sPLA_2$, secreted PLA_2; TEWL, trans-epidermal water loss; TG, transgenic; TPA, 12-*O*-tetradecanoylphorbol-13-acetate.

The epidermis is a highly organized stratified epithelium consisting of basal, spinous, granular, and cornified keratinocyte layers. Survival in a terrestrial dry environment requires an adapted permeability barrier for regulated permeation of water and electrolytes in the stratum corneum (SC). Corneocytes are embedded in a lipid-rich extracellular matrix that forms lamellar membranes composed of ceramides, cholesterol, and fatty acids in an acidic environment (Elias et al., 2008). Perturbation of cutaneous lipid metabolism variably and often profoundly affects SC barrier or keratinocyte homeostasis, leading to skin disorders such as ichthyosis, psoriasis, atopic dermatitis, and cancer (Jobard et al., 2002; Vasireddy et al., 2007).

Linoleic acid (LA; C18:2), by far the most abundant polyunsaturated fatty acid (PUFA) in the SC, is esterified to the ω-hydroxyl group of

K. Yamamoto's present address is Faculty of Bioscience and Bioindustry, Tokushima University, Tokushima 770-8506, Japan.

The Rockefeller University Press $30.00
J. Exp. Med. 2015 Vol. 212 No. 11 1901–1919
www.jem.org/cgi/doi/10.1084/jem.20141904

The Journal of Experimental Medicine

ceramides, which, along with ultra-long-chain fatty acids, are essential for formation of the cornified lipid envelope (Elias et al., 2014). Fatty acids are also important for SC acidification (Mao-Qiang et al., 1996; Fluhr et al., 2001, 2004). Dysregulated production of PUFA- or lysophospholipid-derived lipid mediators can be linked to skin disorders including alopecia, inflammation, and cancer (Nagamachi et al., 2007; Inoue et al., 2011). Release of fatty acids and lysophospholipids from phospholipids is catalyzed by phospholipase A_2 (PLA_2) enzymes, which are classified into several families (Murakami et al., 2011). However, the roles of PLA_2-driven lipid products in epidermal homeostasis and diseases are still not well understood.

The secreted PLA_2 ($sPLA_2$) family consists of 11 members with distinct localizations and substrate specificities (Murakami et al., 2011, 2015). Recent gene targeting of $sPLA_2$s has revealed their distinct roles in various biological events, such as immunity, host defense, atherosclerosis, metabolic disorders, and reproduction (Labonté et al., 2006; Henderson et al., 2007; Escoffier et al., 2010; Sato et al., 2010, 2014; Ait-Oufella et al., 2013; Miki et al., 2013; Taketomi et al., 2013; Boudreau et al., 2014; Pernet et al., 2014). In skin biology, $sPLA_2$s have been suggested to supply bulk fatty acids for formation of the SC acid mantle (Fluhr et al., 2004; Hachem et al., 2005), an idea that stems primarily from the finding that SC acidity is perturbed by nonspecific $sPLA_2$ inhibitors (Mao-Qiang et al., 1996; Fluhr et al., 2001). Furthermore, transgenic (TG) mice overexpressing group IIA (PLA2G2A) or group X (PLA2G10) $sPLA_2$ develop skin abnormalities (Grass et al., 1996; Mulherkar et al., 2003; Yamamoto et al., 2011b). However, the findings that the C57BL/6 mouse strain lacks PLA2G2A due to a natural mutation (MacPhee et al., 1995) and that endogenous PLA2G10 is located in hair follicles (Yamamoto et al., 2011b) cast doubt on the intrinsic roles of these $sPLA_2$s in the epidermis. Overall, it remains unclear whether $sPLA_2$ indeed regulates epidermal lipid processing, and if so, which $sPLA_2$ isoform is important, which lipid species serve as its substrates and products, and how $sPLA_2$-driven lipid metabolism affects skin homeostasis and diseases.

It has recently been reported that group IIF $sPLA_2$ (PLA2G2F), a functionally orphan $sPLA_2$, is expressed in the skin and that its genetic deletion perturbs SC acidification and delays barrier recovery (Ilic et al., 2014; Man et al., 2014). We now show that PLA2G2F is a bona fide epidermal $sPLA_2$ that controls keratinocyte differentiation, hyperproliferation, and function by mobilizing unique lipid products rather than by supplying fatty acids as a whole. Aberrant PLA2G2F expression is associated with epidermal hyperplasia in skin inflammation and cancer. Our results highlight a previously unrecognized $sPLA_2$-driven lipid pathway underlying epidermal-hyperplasic diseases.

RESULTS

PLA2G2F is preferentially expressed in the suprabasal epidermis

We took advantage of epidermal-hyperplasic *PLA2G10*$^{tg/+}$ mice (Yamamoto et al., 2011b) to identify particular lipase-related genes whose expression levels were altered in TG skin compared with control skin and whose in vivo functions are currently unknown. Microarray gene profiling revealed that several lipase-related genes showed increased expression in *PLA2G10*$^{tg/+}$ skin (Table S1). We were interested in *Pla2g2f*, as it was by far the most abundant $sPLA_2$ in control C57BL/6 skin and was increased in hyperplasic *PLA2G10*$^{tg/+}$ skin (Fig. 1 A), a finding that was verified by Northern blotting (Fig. 1 A, inset) and immunohistochemistry (Fig. 1 B). In control skin (P25), the outermost layer of the epidermis was stained with anti-PLA2G2F, but not the control antibody, whereas PLA2G2F staining in *PLA2G10*$^{tg/+}$ skin was more intense and distributed in the thickened epidermis and cysts (Fig. 1 B).

Quantitative RT-PCR demonstrated preferential expression of *Pla2g2f* in the skin (and only at trace levels in the small and large intestines) in C57BL/6 mice (Fig. 1 C). Developmental expression of *Pla2g2f* in mouse skin was far greater than that of other $sPLA_2$s, gradually increasing before birth to reach a maximum level by postnatal day 5 (P5; Fig. 1 D). Separation of the epidermis and hair follicles (P8) by laser-capture microdissection followed by quantitative RT-PCR revealed the expression of *Pla2g2f* in the epidermis rather than in hair follicles, whereas that of other $sPLA_2$s was low or undetectable in both compartments (Fig. 1 E). In situ hybridization confirmed the epidermal location of *Pla2g2f*, which was already detectable at embryonic day 14.5 (E14.5) when epidermal morphogenesis had started (Fig. 1 F). Confocal microscopy of mouse skin showed that PLA2G2F was colocalized with loricrin (a cornified and granular layer marker) and keratin 1 (a granular and spinous layer marker), but not with keratin 5 (a basal layer marker; Fig. 1 G), indicating that PLA2G2F is located in differentiated keratinocytes.

As in mouse skin, *PLA2G2F* was the most abundant $sPLA_2$ in normal human skin, although *PLA2G2A* was also expressed at a relatively low level (Fig. 1 H). Expression of *PLA2G2F*, but not that of *PLA2G2A*, tended to be higher in the psoriasiform skin that expressed higher levels of the psoriasis-associated genes *S100A9*, *IL17A*, and *IL22* (Fig. 1 H). In humans, PLA2G2F immunoreactivity was distributed in the uppermost region of normal skin and increased in the thickened epidermis of psoriasiform skin (Fig. 1 I). Thus, PLA2G2F is a major $sPLA_2$ expressed in the epidermis across species, and its expression increases during epidermal hyperplasia.

Pla2g2f$^{tg/+}$ mice display alopecia and psoriasis-like epidermal hyperplasia

To assess the potential in vivo roles of PLA2G2F, we generated *Pla2g2f*$^{tg/+}$ mice on a C57BL/6 background (Fig. 2 A). *Pla2g2f* expression was elevated in various tissues of *Pla2g2f*$^{tg/+}$ mice relative to WT mice, with a ∼5-fold increase in the TG skin (Fig. 2 B). *Pla2g2f*$^{tg/+}$ mice were born normally, showed no early mortality, were fertile, and had normal serum biomedical parameters (unpublished data).

Pla2g2f$^{tg/+}$ displayed robust skin abnormalities with apparent hair loss at 3–4 wk of age (Fig. 2 C), as seen in *PLA2G10*$^{tg/+}$ mice (Yamamoto et al., 2011b). The dorsal skin of *Pla2g2f*$^{tg/+}$

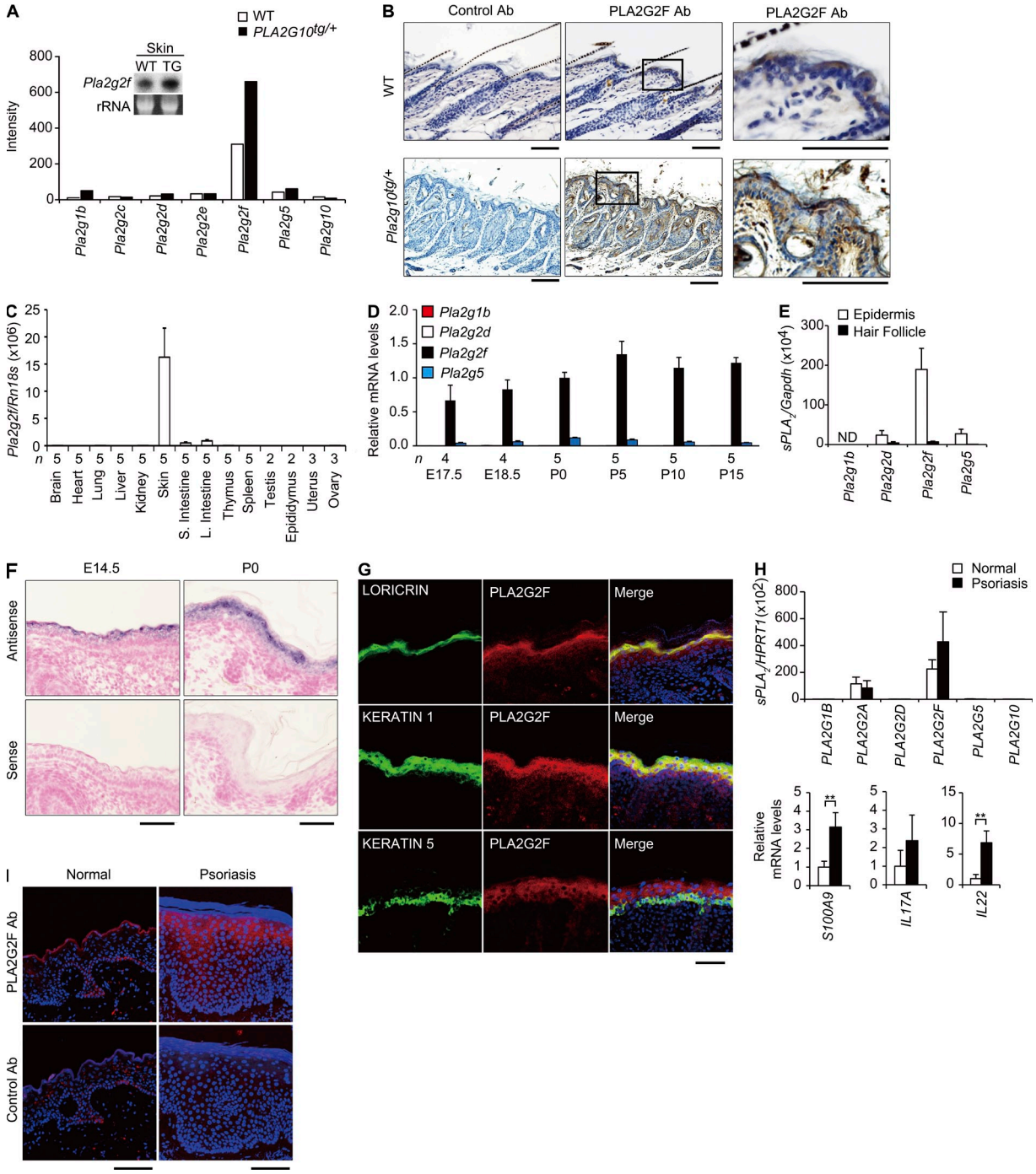

Figure 1. PLA2G2F is expressed in the suprabasal epidermis. (A) Expression of sPLA$_2$s in *PLA2G10*$^{tg/+}$ (TG) and WT skins at P25, as evaluated by microarray. (inset) Northern blotting of *Pla2g2f*, with ribosomal RNA (rRNA) in an agarose gel with ethidium bromide as a control. (B) Immunohistochemistry of PLA2G2F in *PLA2G10*$^{tg/+}$ and WT skins at P25 (bars, 100 µm). Boxes (middle) are magnified on the right. (C) Quantitative RT-PCR of *Pla2g2f* in various tissues of 8-wk-old C57BL/6 mice. (D) Quantitative RT-PCR of sPLA$_2$s in developmental skins of C57BL/6 mice, with expression of *Pla2g2f* at P0 as 1. (E) Microdissection followed by quantitative RT-PCR of sPLA$_2$s in the epidermis (n = 5) and hair follicles (n = 6) of C57BL/6 mice at P8. (F) In situ hybridization of C57BL/6 skin with an antisense or sense probe for *Pla2g2f* (bar, 50 µm). (G) Confocal immunofluorescence microscopy of PLA2G2F (*red*), keratinocyte markers (*green*) and their merged images (*yellow*) in newborn C57BL/6 skin (bar, 100 µm). (H) Quantitative RT-PCR of sPLA$_2$s and psoriasis markers in normal and psoriatic human skins, with expression in normal skin as 1 (n = 7). (I) Immunohistochemistry of PLA2G2F (*red*) in human normal and psoriatic skins, with DAPI counterstaining (blue; bar, 100 µm). Data are from one experiment (A, E, and H) or are representative of two experiments (C, D, and A [inset]; mean ± SEM; *, P < 0.05; **, P < 0.01). Images are representative of two experiments (B, F, G, and I). ND, not detected.

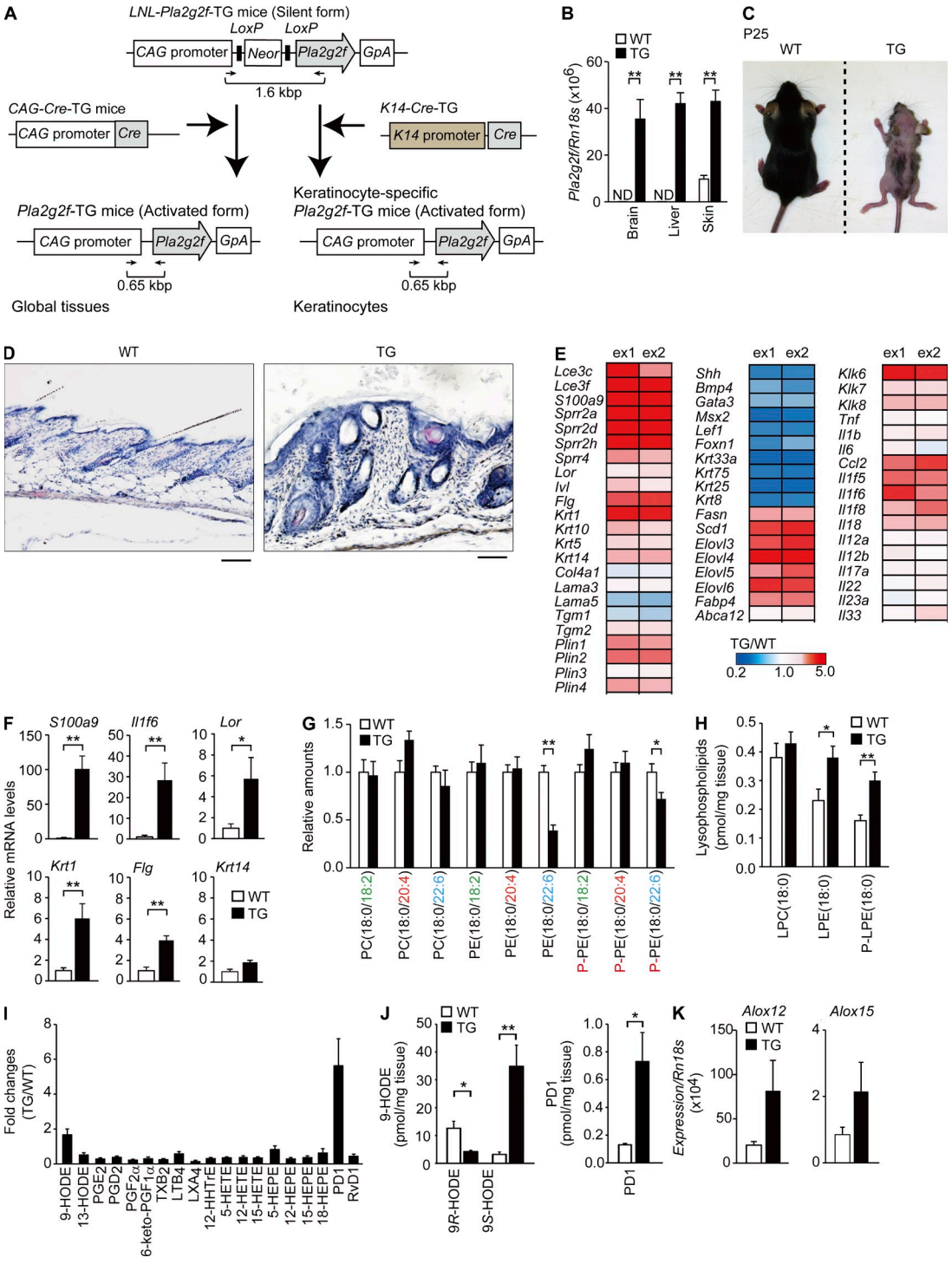

Figure 2. Psoriasis-like epidermal hyperplasia in *Pla2g2f*$^{tg/+}$ mice. (A) Generation of *Pla2g2f*$^{tg/+}$ mice. Mouse *Pla2g2f* cDNA was inserted into the pCALNL5 vector. The plasmid, containing the transgene downstream of a neomycin cassette (*Neo*^{r}) with *LoxP* sites at both ends, was excised at the HindIII and SalI sites to produce a 6-kb *CAG-LoxP-Neo*^{r}*-LoxP-Pla2g2f* (*LNL-Pla2g2f*) fragment. After removal of the *Neo*^{r} cassette by Cre recombinase, a 1.6-kb fragment amplified from the silent form (*LNL-Pla2g2f*$^{tg/+}$) was shifted to a 0.65-kb fragment amplified from the active form (*Pla2g2f*$^{tg/+}$). (B) Quantitative RT-PCR of *Pla2g2f* in *Pla2g2f*$^{tg/+}$ (TG) and WT tissues at P25 ($n = 5$). (C) Gross appearance of *Pla2g2f*$^{tg/+}$ (TG) and WT mice. (D) Hematoxylin-eosin staining of TG and WT skin sections at P25 (bar, 100 µm). (E) Microarray gene profiling of TG versus WT skins at P25. Results are from two experiments (ex1 and ex2). The heat maps are globally normalized for all genes shown in each panel, and the color code shows signal intensity. (F) Quantitative RT-PCR of keratinocyte marker genes in TG and WT skins at P25, with expression in WT skin as 1 ($n = 6$). (G–K) ESI-MS of phospholipids ($n = 5$; G), lysophospholipids ($n = 5$; H), PUFA metabolites ($n = 6$; I), and 9-HODEs and PD1 ($n = 6$; I and J) in WT and TG skins at P25. Relative amounts, with values for WT skin as 1

mice at P25 exhibited epidermal and sebaceous gland hyperplasia, hair follicle distortion and cyst formation, with the uppermost layer of the epidermis displaying hyperkeratosis with a highly thickened SC (Fig. 2 D). Microarray gene profiling (Fig. 2 E and Table S2) and quantitative RT-PCR (Fig. 2 F) supported the overall tendency for epidermal and sebaceous gland hyperplasia, as well as alopecia in *Pla2g2f*$^{tg/+}$ skin. A dramatic increase in the expression of *S100a9*, a marker of hyperproliferated and activated keratinocytes in psoriasis (Schonthaler et al., 2013), or *Il1f6*, which encodes the psoriasis-related keratinocyte cytokine IL-36α (Tortola et al., 2012; Fig. 2, E and F), indicated that the epidermal hyperplasia in *Pla2g2f*$^{tg/+}$ mice has some features of psoriasis. We also generated skin-specific *K14-Pla2g2f*$^{tg/+}$ mice and obtained similar results (unpublished data), implying that PLA2G2F has a skin-intrinsic role. The smaller body size of *Pla2g2f*$^{tg/+}$ mice at P25 might be a result of up-regulation of thermogenic processes for temperature maintenance at the expense of fuel economy, an event often observed in hairless mice (Smith et al., 2000).

Although the phenotypes observed in sPLA$_2$ TG mice may not necessarily reflect the intrinsic functions of endogenous sPLA$_2$s, they are useful for screening their potential in vivo substrates (phospholipids) and products (lysophospholipids, fatty acids, and their metabolites; Yamamoto et al., 2011a, b). Electrospray ionization mass spectrometry (ESI-MS) of skin lipids revealed that diacyl and plasmalogen (P-) forms of phosphatidylethanolamine (PE) with docosahexaenoic acid (DHA; C22:6), but not other phospholipids, were significantly reduced in *Pla2g2f*$^{tg/+}$ mice relative to WT mice (Fig. 2 G). Accordingly, there were concomitant increases in the acyl and plasmalogen forms of lysophosphatidylethanolamine (LPE and P-LPE, respectively), but not lysophosphatidylcholine (LPC), in TG skin (Fig. 2 H). These results suggest that the overexpressed PLA2G2F hydrolyzes PE and P-PE species with DHA as preferred substrates rather than acting on all phospholipids randomly. Of the oxygenated PUFA metabolites, the level of protectin D1 (PD1), a DHA metabolite that facilitates survival and renewal of epithelial cells (Serhan et al., 2006, 2014, 2015; Bazan et al., 2010), but not arachidonic acid (AA; C20:4)–derived or eicosapentaenoic acid (EPA; 20:5)–derived metabolites, was noticeably increased in *Pla2g2f*$^{tg/+}$ skin (Fig. 2, I and J). Although the levels of LA-containing phospholipids were similar in both genotypes (Fig. 2 G), the level of 9*S*-hydroxyoctadecadienoic acid (HODE), a LA metabolite that activates keratinocytes (Hattori et al., 2008), was increased in TG skin relative to control (Fig. 2, I and J). Cutaneous expression of *Alox12* and *Alox15*, which encode lipoxygenases (LOXs) that convert LA and DHA to 9*S*-HODE and PD1, respectively, was substantially higher in *Pla2g2f*$^{tg/+}$ mice than in WT mice (Fig. 2 K). These results suggest that the increases of these metabolites are caused by an increased supply of PUFA precursors and/or the increased expression of PUFA-metabolizing LOXs in TG skin. Thus, among the potential PLA$_2$-driven lipids detected so far, LPE, P-LPE, PD1, and 9*S*-HODE appear to be specific metabolites that are increased in *Pla2g2f*$^{tg/+}$ skin. We therefore focused on these lipid metabolites in subsequent studies.

Pla2g2f$^{-/-}$ mice have fragile SC

To investigate the physiological roles of endogenous PLA2G2F in vivo, we generated *Pla2g2f*$^{-/-}$ mice (Fig. 3 A). Heterozygous mice carrying a mutated *Pla2g2f* allele (*Pla2g2f*$^{+/-}$) were backcrossed onto a C57BL/6 background ($n > 12$). Successful ablation of the *Pla2g2f* gene was confirmed by PCR genotyping from tail biopsy specimens (unpublished data) and by absence of its protein in the isolated SC (Fig. 3 B) and skin tissue (Fig. 3 C) of *Pla2g2f*$^{-/-}$ mice. Skin expression of other sPLA$_2$s was unaffected by *Pla2g2f* ablation (unpublished data). The ratio of genotypes of heterozygous male and female offspring exhibited Mendelian proportions, and homozygous-null mice were indistinguishable from WT mice in terms of survival, fertility, behavior, and serum parameters (unpublished data).

A recent study has reported that PLA2G2F participates in formation of the SC barrier and acidity (Ilic et al., 2014). In our studies, *Pla2g2f*$^{-/-}$ mice from the embryonic to adult (8-wk-old) stages appeared grossly normal, and transmission electron microscopy revealed no ultrastructural abnormality in the dorsal skin of adult *Pla2g2f*$^{-/-}$ mice (unpublished data). Nonetheless, we noticed several unusual ultrastructural features in the SC of abdominal skin in *Pla2g2f*$^{-/-}$ mice. In contrast to the well-organized SC structure with 7–8 cornified layers interspaced by lipid matrices in the abdominal skin of *Pla2g2f*$^{+/+}$ mice, the SC of *Pla2g2f*$^{-/-}$ mice had only a few layers with signs of disorganized desmosomes, decreased stratification, accelerated desquamation, and edematous intercorneous spaces (Fig. 3 D). Trans-epidermal water loss (TEWL; Fig. 3 E) and cutaneous pH (Fig. 3 F) were higher in the abdominal, but not dorsal, skin of *Pla2g2f*$^{-/-}$ mice than that of *Pla2g2f*$^{+/+}$ mice, indicating that the mutant mice have perturbation of the SC barrier and acidification only in the abdominal skin. In comparison, deficiency of other sPLA$_2$s did not affect TEWL signficantly (Fig. 3 E). Although tape-stripped corneocytes from *Pla2g2f*$^{-/-}$ dorsal skin appeared normal in shape, short-term sonication resulted in more rapid collapse of *Pla2g2f*$^{-/-}$ cells than *Pla2g2f*$^{+/+}$ cells (Fig. 3 G), suggesting that *Pla2g2f*$^{-/-}$ mice have a fragile SC. Likely as a result of this SC fragility, epidermal layers beneath the SC of *Pla2g2f*$^{-/-}$ abdominal skin became thickened (Fig. 3 D), which may reflect a compensatory adaptation to the SC barrier defect, an event often seen in skin disorders characterized by SC abnormalities.

ESI-MS revealed that the levels of ceramides, which are prerequisite for the SC barrier, and fatty acids, which are

(G and I), or quantified amounts per milligram of tissue (H and J) are shown. (K) Quantitative RT-PCR of LOXs in TG and WT skins at P25 ($n = 6$). Data are representative of two (B, F, J, and K) or three (G–I) experiments (mean ± SEM; *, $P < 0.05$; **, $P < 0.01$). Images are representative of three experiments (C and D). ND, not detected. HETE, hydroxyeicosatetraenoic acid; HHTrE, hydroxyheptadecatrienoic acid; LT, leukotriene; LX, lipoxin; TX, thromboxane.

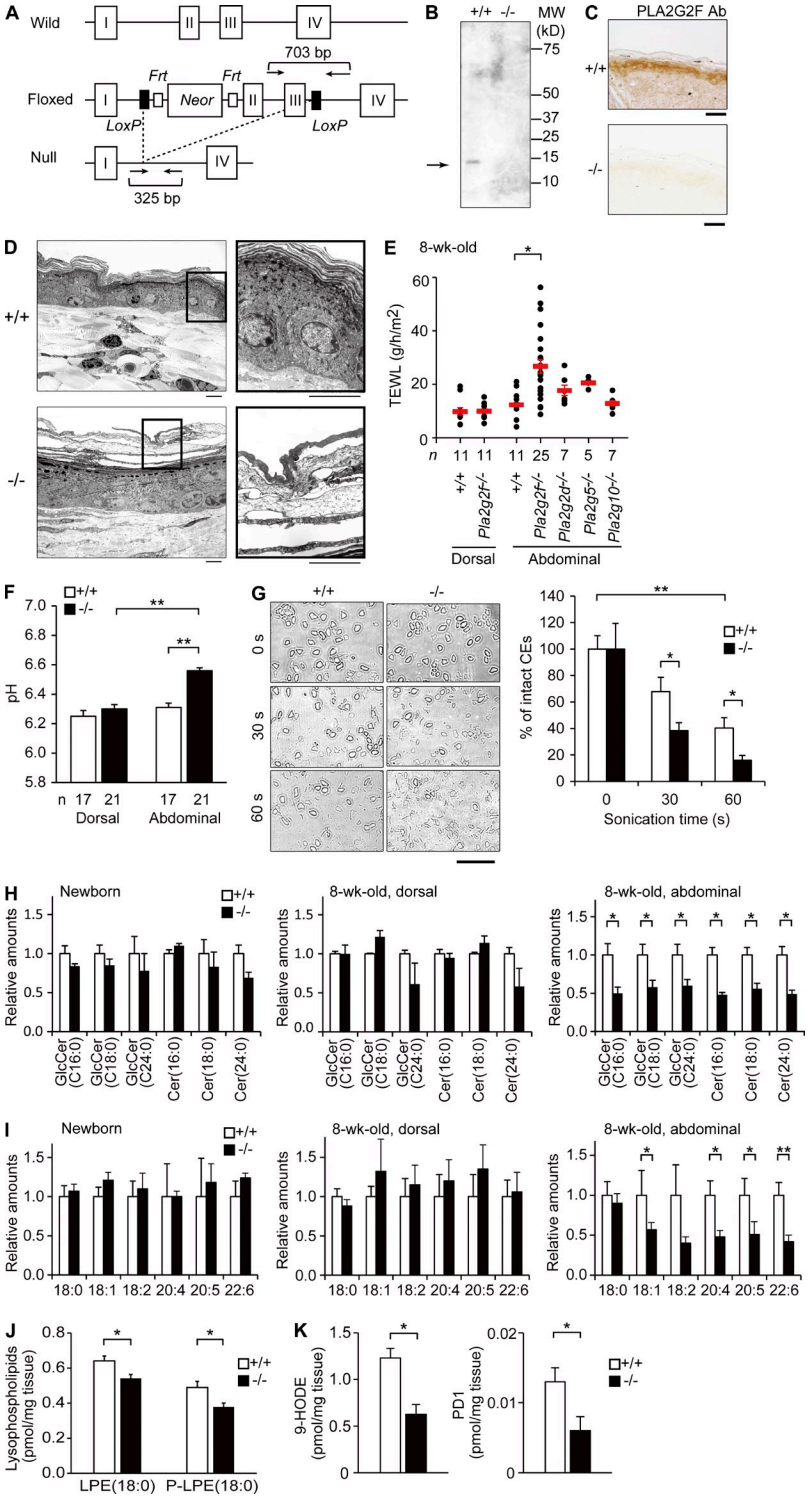

Figure 3. SC abnormalities in *Pla2g2f*$^{-/-}$ mice. (A) Generation of *Pla2g2f*$^{-/-}$ mice. The *Pla2g2f*-targeting vector was constructed with the *Neo*^{r} gene that was inserted between exons 1 and 2 of the *Pla2g2f* gene. After mating with *CAG-Cre*$^{tg/+}$ mice, the exons 2 and 3 plus the *Neo*^{r} casette were removed to generate *Pla2g2f*-null mice. Arrows indicate primer positions for genotyping. (B) Immunoblotting of PLA2G2F protein in the SC of adult *Pla2g2f*$^{+/+}$ and *Pla2g2f*$^{-/-}$ mice. (C) Immunohistochemistry of PLA2G2F in *Pla2g2f*$^{+/+}$ and *Pla2g2f*$^{-/-}$ skins at P0 (bars, 100 µm). (D) Transmission electron microscopy of abdominal skins of *Pla2g2f*$^{+/+}$ and *Pla2g2f*$^{-/-}$ mice (bar, 5 µm). Boxes are magnified on the right. (E) TEWL of dorsal and abdominal skins from various $sPLA_2$-null or WT mice. (F) pH of dorsal and abdominal skins from *Pla2g2f*$^{+/+}$ and *Pla2g2f*$^{-/-}$ mice. (G) Microscopic images of corneocytes (CEs) after sonication for the indicated periods (bar, 50 µm). (right) Percentages of intact cells ($n = 7$). (H and I) ESI-MS of ceramides ($n = 6$; H) and fatty acids ($n = 6$; I) in newborn and adult (dorsal and abdominal) *Pla2g2f*$^{+/+}$ and *Pla2g2f*$^{-/-}$ skins, the values for WT skin being 1. (J and K) ESI-MS of LPE and P-LPE (J) or 9-HODE and PD1 (K) in abdominal *Pla2g2f*$^{+/+}$ and *Pla2g2f*$^{-/-}$ skins ($n = 6$). Data are representative from two experiments (G–K) or compiled from three experiments (E and F; mean ± SEM; *, $P < 0.05$; **, $P < 0.01$). Representative images of one or two experiments are shown (B, C, D, and G). Cer, ceramide; GlcCer, glucosylceramide.

important for SC acidification, were not altered in newborn or adult dorsal skin, whereas most of them were significantly reduced in the adult abdominal skin of *Pla2g2f*$^{-/-}$ mice compared with *Pla2g2f*$^{+/+}$ mice (Fig. 3, H and I). Collectively, these data suggest that although epidermal differentiation and SC barrier formation occur almost normally in *Pla2g2f*$^{-/-}$ mice under normal conditions, the SC of the null mice is vulnerable to mechanical or other environmental stresses (e.g., exposure to floor friction), leading to collapse of the abdominal SC and thereby perturbation of skin barrier and acidity, with concomitant decreases in multiple ceramide and fatty acid species. Notably, regardless of the distinct skin locations,

the levels of LPE, P-LPE, 9-HODE, and PD1, which were higher in *Pla2g2f*$^{tg/+}$ mice (Fig. 2, H–J), were reciprocally lower in *Pla2g2f*$^{-/-}$ mice than in controls (Fig. 3, J and K). Therefore, we speculated that the altered metabolism of particular lipid products, rather than the hydrolysis of skin phospholipids as a whole, may underlie the mechanistic actions of PLA2G2F.

Abnormal differentiation and activation of *Pla2g2f*$^{-/-}$ keratinocytes in culture

To explore the expression and function of PLA2G2F further, we used keratinocytes in primary culture. An epidermal Ca^{2+} gradient regulates keratinocyte differentiation and barrier function (Tu et al., 2012). Indeed, Ca^{2+} treatment of *Pla2g2f*$^{+/+}$ keratinocytes resulted in marked induction of various markers of keratinocyte differentiation or activation (*Krt14*, *Krt1*, *Lor*, *Il1f6*, and *S100a9*), as well as *Pla2g2f* (Fig. 4 A). Importantly, this Ca^{2+}-induced response was markedly impaired in *Pla2g2f*$^{-/-}$ keratinocytes (Fig. 4 A). Microarray analysis using *Pla2g2f*$^{+/+}$ and *Pla2g2f*$^{-/-}$ keratinocytes further supported this view, where the expression levels of many if not all Ca^{2+}-induced genes were down-regulated in *Pla2g2f*$^{-/-}$ cells (Fig. 4 B and Table S3). Consistent with these observations, treatment of WT keratinocytes with a $sPLA_2$ inhibitor (LY315920 derivative) that broadly inhibits $sPLA_2$s (Oslund et al., 2008), but not its placebo, suppressed *S100a9* induction (Fig. 4 C). The impaired Ca^{2+}-driven keratinocyte activation in *Pla2g2f*$^{-/-}$ culture was restored by recombinant mouse PLA2G2F dose-dependently or by 9*S*-HODE, a potential PLA2G2F-driven product (Fig. 4 D). P-LPE also increased Ca^{2+}-induced *S100a9* and *Krt1* expression in *Pla2g2f*$^{+/+}$ cells and restored it in *Pla2g2f*$^{-/-}$ cells, whereas 10*S*,17*S*-dihydroxy-DHA (10,17-diHDoHE, a commercially available PD1 stereoisomer) augmented the expression of these genes in *Pla2g2f*$^{+/+}$, but not in *Pla2g2f*$^{-/-}$, cells (Fig. 4 E).

It has been reported that differentiated keratinocytes secrete lipids (e.g., ceramides, cholesterol, and phospholipids) from lamellar granules for extracellular hydrolysis and that this extracellular phospholipid pool may serve as a substrate for $sPLA_2$ (Fluhr et al., 2004). Lipidomics studies of keratinocyte supernatants in serum-free culture revealed that WT keratinocytes did secrete phospholipids, particularly PE (Fig. 4 F), whereas the release of phosphatidylcholine (PC) was small (not depicted). The release of phospholipids was markedly lower in *Pla2g2f*$^{-/-}$ than in *Pla2g2f*$^{+/+}$ cultures (Fig. 4 F), suggesting that this event relies on proper PLA2G2F-dependent keratinocyte differentiation. Probably because of the impaired substrate secretion or keratinocyte differentiation, the release of LPE, P-LPE, LA, DHA, and 9-HODE was also compromised in *Pla2g2f*$^{-/-}$ cells, whereas AA release was relatively low and LPC release was similar in both genotypes (Fig. 4 G). The failure to detect PD1 despite the robust release of DHA in WT culture suggests that the expression of LOXs responsible for the conversion of DHA to PD1 is low in keratinocytes or that its production requires the co-presence of other cell types in vivo. Thus, 9-HODE or LPE species may represent particular lipid metabolites responsible for PLA2G2F-dependent keratinocyte differentiation or activation.

As in mouse keratinocytes, the expression of *PLA2G2F,* but not other $sPLA_2$s, was induced in human keratinocytes after Ca^{2+} treatment (Fig. 4 H). A *PLA2G2F*-specific, but not a scramble, siRNA reduced the Ca^{2+}-induced expression of *KRT1*, *LOR*, and *S100A9*, as well as *PLA2G2F* (Fig. 4 I). Thus, the role of PLA2G2F in keratinocytes may also be relevant in human epidermis.

Substrate selectivity of PLA2G2F

To better address the substrate specificity of PLA2G2F, we performed in vitro enzymatic assays using recombinant mouse PLA2G2F (Singer et al., 2002). Given that $sPLA_2$s act on extracellular phospholipids such as lipoproteins and microparticles (Boudreau et al., 2014; Sato et al., 2014), we incubated the serum-free culture medium of WT keratinocytes with PLA2G2F to examine the hydrolysis of phospholipids secreted from keratinocytes. After incubation, there was robust production of P-LPE species in comparison with other lysophospholipids (Fig. 5 A), indicating that PLA2G2F preferentially hydrolyzes P-PE secreted from the cells. Upon addition of a low dose of PLA2G2F to skin-extracted lipids, P-PE species containing DHA were preferentially hydrolyzed to yield P-LPE, whereas this substrate selectivity was apparently lost when a higher dose of PLA2G2F was added to the assay, with most species of PE with different fatty acid species being hydrolyzed to various degrees (Fig. 5, B–D). Taking the in vitro and in vivo results altogether, it appears that PLA2G2F has a substrate preference for DHA-containing P-PE secreted from keratinocytes under physiological conditions.

PLA2G2F promotes epidermal hyperplasia in psoriasis and contact dermatitis

Given the psoriasis-like phenotype in the skin of *Pla2g2f*$^{tg/+}$ mice (Fig. 2) and the impaired induction of psoriasis-associated genes in *Pla2g2f*$^{-/-}$ keratinocytes (Fig. 4), we next examined whether endogenous PLA2G2F participates in relevant skin pathologies. Psoriasis, one of the most common chronic inflammatory skin diseases, is characterized by epidermal hyperplasia (acanthosis) caused by aberrant proliferation and differentiation of keratinocytes, scaling, erythematous plaque formation, and infiltration of immune cells such as Th17 cytokine-producing lymphocytes (Lowes et al., 2014). In a model of imiquimod (IMQ)-induced psoriasis (Tortola et al., 2012), IMQ challenge onto the ears of WT mice elicited dermal swelling and acanthosis, accompanied by marked increases of *Pla2g2f* mRNA and its protein in the thickened epidermis, where PLA2G2F was colocalized with loricrin that was distributed diffusely throughout the suprabasal layers (Fig. 6, A and B). The IMQ-induced ear edema and epidermal thickening (Fig. 6, C–E) as well as IMQ-induced expression of various keratinocyte markers (*S100a9*, *Defb3*, *Lor*, *Tnf*, *Il6, Il1f6*, and *Il1f9*; Fig. 6 F) were significantly less marked in *Pla2g2f*$^{-/-}$ mice than in *Pla2g2f*$^{+/+}$ mice. However, dermal migration of neutrophils, macrophages, and γδT cells expressing IL-17A

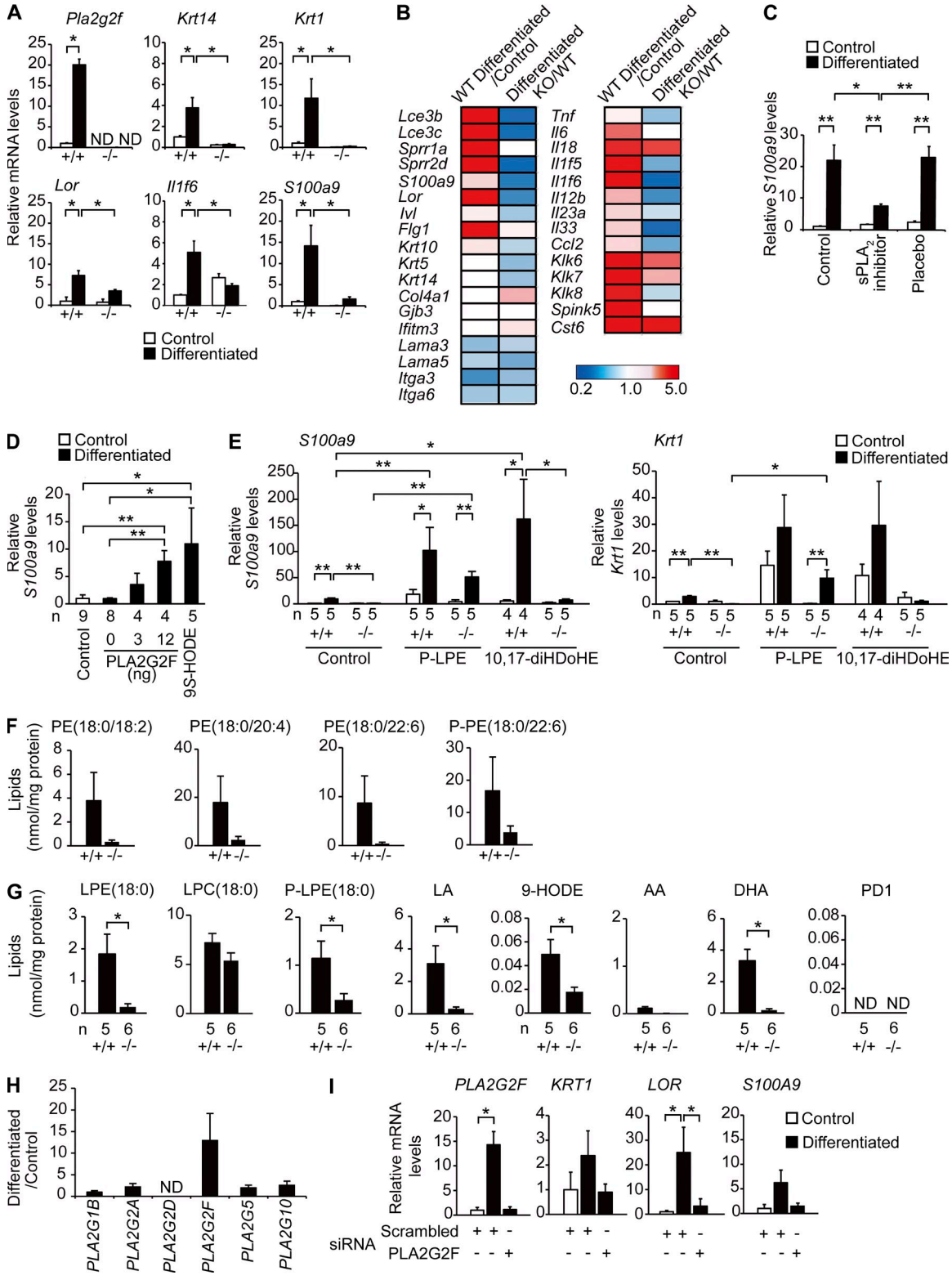

Figure 4. Impaired differentiation and activation of *Pla2g2f*$^{-/-}$ keratinocytes. (A) Quantitative RT-PCR of *Pla2g2f* and keratinocyte markers in *Pla2g2f*$^{+/+}$ and *Pla2g2f*$^{-/-}$ keratinocytes after culture for 2 d with (differentiated) or without (control) 1 mM $CaCl_2$ ($n = 5$). (B) Microarray gene profiling of *Pla2g2f*$^{+/+}$ (WT) and *Pla2g2f*$^{-/-}$ (KO) keratinocytes. Ratios of differentiated to control cultures in WT cells and those of KO to WT cells after differentiation are shown. The heat maps are globally normalized for all genes and the color code shows signal intensity. (C–E) Quantitative RT-PCR of *S100a9* or *Krt1* after 2-d culture of WT cells with 10 nM $sPLA_2$ inhibitor or placebo ($n = 5$; C), KO cells with various doses of PLA2G2F or 10 nM 9*S*-HODE ($n = 5$; D),

or IL-22 was not affected by *Pla2g2f* deficiency (unpublished data), implying that the primary defects caused by *Pla2g2f* ablation are specific for keratinocytes.

Lipidomics revealed that P-LPE was markedly increased after IMQ challenge and significantly more abundant in $Pla2g2f^{+/+}$ skin than in $Pla2g2f^{-/-}$ skin, whereas neither LPE nor LPC differed regardless of IMQ challenge or genotype (Fig. 6 G). 9-HODE and PD1 were also markedly elevated in IMQ-treated skin relative to vehicle-treated skin, yet unlike in normal skin (Fig. 3 K), their levels were not affected by *Pla2g2f* deficiency (Fig. 6 G), probably because *Alox15b* expression was equally elevated in the psoriatic skins of both genotypes (Fig. 6 F) or because other PLA_2s in massively infiltrated leukocytes might be responsible for their production. AA-derived eicosanoids were also increased in IMQ-treated skin, with no influence by *Pla2g2f* deficiency (Fig. 6 G). Thus, P-LPE is the only metabolite that correlates with *Pla2g2f* expression in psoriatic skin.

To circumvent the bias arising from the presence of other cell types in the psoriatic skin in vivo, we again took advantage of primary keratinocytes. We found that IL-22, a psoriasis-associated Th17 cytokine (Lowes et al., 2014), induced *Pla2g2f* expression markedly (Fig. 7 A) and that the induction of *S100a9* and *Il1f6* by Th17 cytokines was abrogated by *Pla2g2f* deficiency (Fig. 7 B). Lipidomics of the culture supernatants revealed attenuated release of P-LPE and 9-HODE in IL-22–treated $Pla2g2f^{-/-}$ cells, whereas PD1 was undetectable even in WT cells (Fig. 7 C). The defective IL-22–induced *S100a9* expression in $Pla2g2f^{-/-}$ cells was partially restored by P-LPE, but not by 9*S*-HODE or the PD1 isomer 10,17-diHDoHE (Fig. 7 D). Moreover, topical application of P-LPE onto the $Pla2g2f^{-/-}$ skin rescued the defective IMQ-induced epidermal hyperplasia (Fig. 7, E and F) and keratinocyte activation (Fig. 7 G) in vivo, whereas LPE, 9-HODE, and 10,17-diHDoHE had no effect (Fig. 7 H). These results suggest that PLA2G2F is induced by IL-22 in keratinocytes and promotes keratinocyte activation by mobilizing P-LPE in psoriasis.

We also evaluated the effects of *Pla2g2f* ablation on hapten-induced contact dermatitis, in which application of dinitrofluorobenzene (DNFB) to abdominal skin followed by a second application of the same antigen to ear skin induced ear swelling (Miki et al., 2013). Expression of *Pla2g2f* mRNA and its protein was markedly elevated in the epidermis of DNFB-challenged WT skin relative to vehicle-treated skin, again being colocalized with loricrin (Fig. 8, A and B). The DNFB-induced ear thickening and epidermal hyperplasia were significantly milder in $Pla2g2f^{-/-}$ mice than in $Pla2g2f^{+/+}$ mice (Fig. 8, C–E). DNFB-induced expression of markers for keratinocytes, but not those for immune cells, was significantly lower in $Pla2g2f^{-/-}$ mice than in $Pla2g2f^{+/+}$ mice (Fig. 8 F), again revealing the keratinocyte-specific effects of *Pla2g2f* ablation. Among the lipid products on which we focused, only P-LPE was increased in DNFB-treated $Pla2g2f^{+/+}$ skin, whereas this event occurred only partially in $Pla2g2f^{-/-}$ skin (Fig. 8 G). Collectively, we conclude that PLA2G2F promotes the aggravation of epidermal hyperplasia in psoriasis and contact dermatitis and that P-LPE represents a particular lipid product that mirrors the epidermal expression and function of PLA2G2F.

PLA2G2F exacerbates skin carcinogenesis

Skin-specific TG mice for mouse PLA2G2A ($K14\text{-}Pla2g2a^{tg/tg}$) are susceptible to a model of chemical carcinogenesis induced by 9,10-dimethylbenz(a)anthracene (DMBA) and 12-*O*-tetradecanoylphorbol-13-acetate (TPA; Mulherkar et al., 2003). Given that PLA2G2F is a major skin $sPLA_2$, we applied DMBA/TPA to $Pla2g2f^{-/-}$ and $Pla2g2f^{+/+}$ mice on a BALB/c background, a strain that is more sensitive to this model of carcinogenesis. *Pla2g2f* expression was induced by TPA in WT keratinocytes (Fig. 9 A) and tended to increase in DMBA/TPA-treated WT skin relative to control skin at 4 wk (Fig. 9 B). At 24 wk, $Pla2g2f^{-/-}$ mice were highly protected from the development of skin tumors, in which epidermal thickening was markedly attenuated (Fig. 9, C and D). PLA2G2F staining in the WT tumor was distributed throughout the thickened epidermis (Fig. 9 E). Although tumor incidence and multiplicity were similar in both genotypes over time (Fig. 9 F), the tumors in $Pla2g2f^{-/-}$ mice were smaller than those in $Pla2g2f^{+/+}$ mice, large tumors (>50 mm^3) being absent at 24 wk (Fig. 9 G), suggesting that *Pla2g2f* deficiency retarded tumor growth. Expression of keratinocyte differentiation, hyperproliferation, or activation markers was lower in $Pla2g2f^{-/-}$ than in $Pla2g2f^{+/+}$ tumors (Fig. 9 H). Moreover, expression of immune cell markers, indicative of tumor infiltration by immune cells, was reduced in $Pla2g2f^{-/-}$ mice (Fig. 9 H), possibly as a result of attenuated tumor progression. Indeed, the lower expression of *Cd206* (Fig. 9 H), a marker of tumor-associated macrophages that accelerate tumor growth (Condeelis and Pollard, 2006), and the reduced infiltration and degranulation of mast cells (Fig. 9 I), which diversely affect cancer (Marichal et al., 2013), may contribute to the reduced tumor size in $Pla2g2f^{-/-}$ mice.

Lipidomics revealed that P-LPE, 9-HODE, and PD1 were markedly increased in the $Pla2g2f^{+/+}$ tumors, whereas these changes were less evident in the $Pla2g2f^{-/-}$ tumors (Fig. 9 J).

or WT and KO cells with 10 nM P-LPE or 10,17-diHDoHE ($n = 5$; E). (F and G) ESI-MS of phospholipids (F) and metabolites (G) in keratinocyte supernatants after differentiation culture for 2 d ($n = 5$). (H) Quantitative RT-PCR of $sPLA_2$s in human keratinocytes. Fold increases after culture for 2 d with 1 mM $CaCl_2$, with that of *PLA2G1B* as 1, are shown ($n = 6$). (I) Quantitative RT-PCR of keratinocyte genes in human keratinocytes that were pretreated with *PLA2G2F* or scrambled siRNA, and then cultured with or without 1 mM $CaCl_2$ for 2 d ($n = 4$). In A, C-E, and I, expression was normalized with *Rn18s*, the values for the control culture being 1. Data are from one experiment (B and C) or are representative of two (H and I) or three (A and D–G) experiments (mean ± SEM; *, $P < 0.05$; **, $P < 0.01$). ND, not detected.

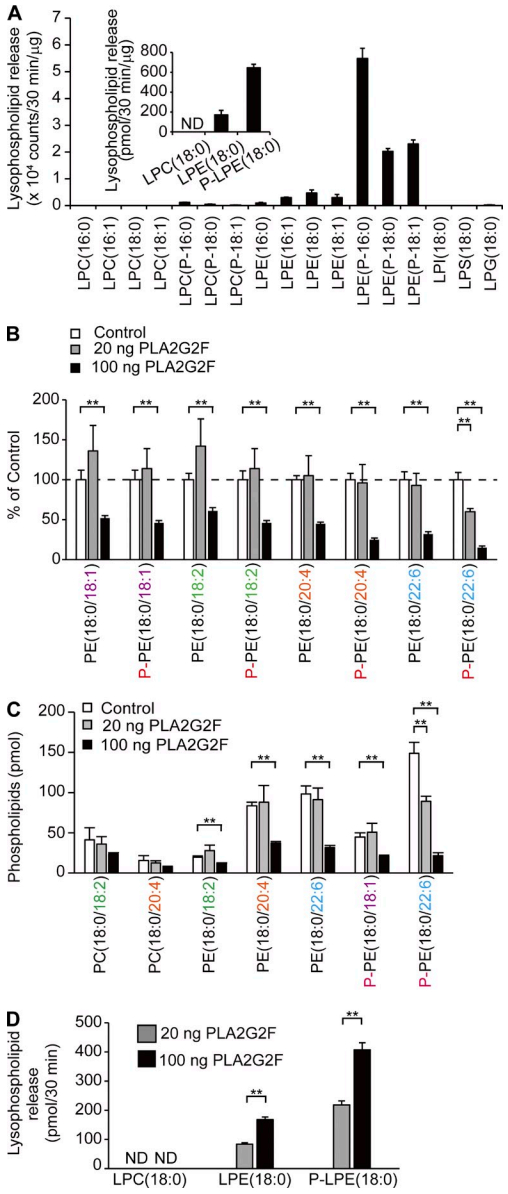

Figure 5. Substrate selectivity of PLA2G2F in vitro. (A) ESI-MS of lysophospholipids after incubation of keratinocyte supernatants with PLA2G2F (20 ng) for 30 min ($n = 5$). (inset) Quantified data ($n = 5$). (B–D) Evaluation of the substrate specificity of PLA2G2F toward phospholipids extracted from mouse skin. After incubation of skin-extracted lipids for 30 min with 20 or 100 ng of PLA2G2F, phospholipids (B and C) and lysophospholipids (D) were analyzed by ESI-MS ($n = 5$). Values represent percentages with the control (no PLA2G2F) as 100% (B) or are quantified values (C and D). Data are representative of two experiments (mean ± SEM; *, $P < 0.05$; **, $P < 0.01$). ND, not detected.

The tumor-associated increases of prostanoids were similar in the two genotypes (Fig. 9 J). Thus, the aforementioned studies show that several lipid metabolites can be affected by PLA2G2F in different experimental settings, with P-LPE appearing as a common PLA2G2F-related biomarker and bioactive metabolite. Collectively, our results suggest that PLA2G2F is an intrinsic skin $sPLA_2$ that contributes to multiple epidermal disorders, including psoriasis, contact dermatitis, and cancer, by driving a unique lipid pathway.

DISCUSSION

Studies over the past decade have revealed the pathophysiological functions of various $sPLA_2$s, as exemplified by group IB, IIA, IID, IIE, III, V, and X $sPLA_2$s acting as digestive, inflammatory or bactericidal, resolving, metabolic, reproductive or anaphylactic, metabolic or Th2-prone, and reproductive or asthmatic $sPLA_2$s, respectively (Labonté et al., 2006; Henderson et al., 2007; Escoffier et al., 2010; Sato et al., 2010, 2014; Ait-Oufella et al., 2013; Miki et al., 2013; Taketomi et al., 2013; Boudreau et al., 2014; Pernet et al., 2014). In this study, we have provided comprehensive insights into PLA2G2F, an orphan $sPLA_2$ whose expression, target substrates and products, and functions in vivo have remained largely unknown. Our results reveal a previously unrecognized role of PLA2G2F, an epidermal $sPLA_2$, in skin homeostasis and diseases and point to this enzyme as a novel drug target for skin disorders characterized by epidermal hyperplasia such as psoriasis and cancer. Therefore, the skin phenotypes observed in TG mice for PLA2G2A (Grass et al., 1996; Mulherkar et al., 2003) or PLA2G10 (Yamamoto et al., 2011b) suggest that these enzymes mimic the intrinsic actions of PLA2G2F when artificially overexpressed in skin, or that endogenous PLA2G2F is up-regulated in the hyperplasic epidermis of these TG mice.

Previous pharmacological studies have suggested the potential role of $sPLA_2$s in SC acidification (Mao-Qiang et al., 1996; Fluhr et al., 2001), and a recent preliminary study using *Pla2g2f*$^{-/-}$ mice showed that this $sPLA_2$ may be involved in this process (Ilic et al., 2014). In the present study, we confirmed that PLA2G2F is a major $sPLA_2$ expressed in the suprabasal epidermis of both mouse and human. In contrast to other $sPLA_2$s that are active at neutral to alkaline pH, PLA2G2F exhibits nearly full activity within a pH range in line with skin acidity (Valentin et al., 1999). Notably, mice null for PLA2G2F, but not for other $sPLA_2$s, have SC abnormalities with perturbed acidity and barrier function, although this phenotype is evident only in the abdominal (but not dorsal or newborn) skin of *Pla2g2f*$^{-/-}$ mice under normal conditions. It is therefore likely that PLA2G2F contributes to SC stability or recovery from SC perturbation in response to environmental stress (e.g., friction against the floor or prolonged exposure to microbiota) rather than to the central program of epidermal differentiation or basal SC barrier function and acidity.

Nevertheless, keratinocytes in culture fail to show proper differentiation and activation when PLA2G2F is ablated genetically or pharmacologically, a phenotype that is partially restored by PLA2G2F or its lipid metabolites. The more profound effects of *Pla2g2f* deficiency on keratinocytes in vitro than in vivo suggest that some mechanisms compensating for the lack of PLA2G2F might exist in vivo, as reported for mice null for several molecules crucial for skin homeostasis (Koch et al., 2000; Gareus et al., 2007). For instance, other (one or more) $sPLA_2$s together with PLA2G2F might be

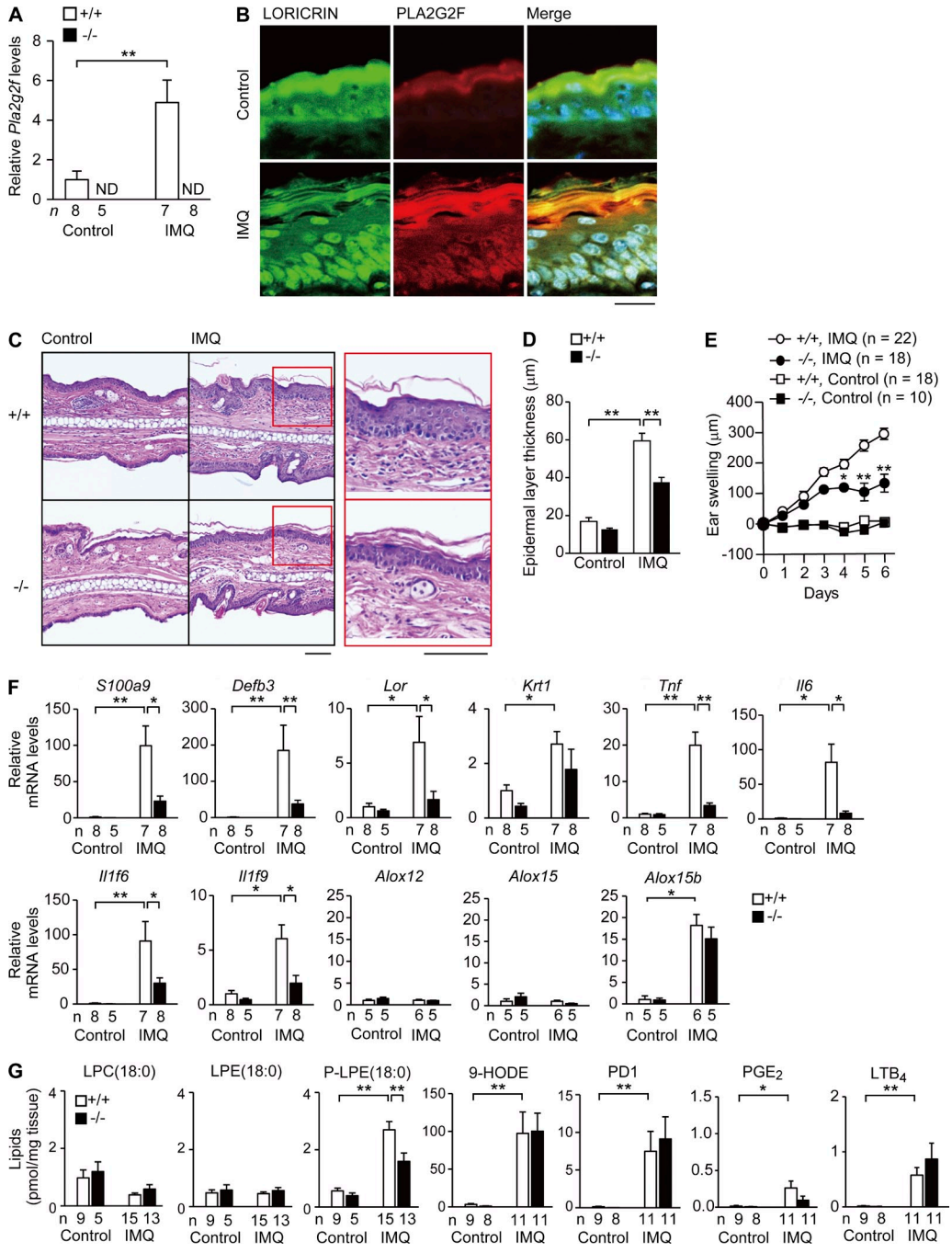

Figure 6. Reduced psoriasis in *Pla2g2f*$^{-/-}$ mice. (A) Quantitative RT-PCR of *Pla2g2f* in *Pla2g2f*$^{+/+}$ and *Pla2g2f*$^{-/-}$ ears with or without (control) IMQ treatment for 6 d. (B) Confocal microscopy of PLA2G2F (red), loricrin (green), and their merged images (yellow) in WT skin on day 6, with DAPI counterstaining (blue; bar, 20 µm). (C) Hematoxylin-eosin staining of *Pla2g2f*$^{+/+}$ and *Pla2g2f*$^{-/-}$ ears on day 6 (bar, 50 µm). Boxes are magnified on the right. (D and E) Epidermal thickness on day 6 ($n = 6$; D) or time-dependent ear swelling (E) of *Pla2g2f*$^{+/+}$ and *Pla2g2f*$^{-/-}$ mice. (F) Quantitative RT-PCR of keratinocyte and immune markers in *Pla2g2f*$^{+/+}$ and *Pla2g2f*$^{-/-}$ ears on day 6. (G) ESI-MS of lipid metabolites in *Pla2g2f*$^{+/+}$ and *Pla2g2f*$^{-/-}$ ears on day 6. In A and F, expression was normalized against *Gapdh*, the value for the control WT group being 1. Data are compiled from two experiments (A and D–G; mean ± SEM; *, $P < 0.05$; **, $P < 0.01$). ND, not detected. Images are representative of two experiments (B and C).

involved in fatty acid release for SC acidification, and deficiency of PLA2G2F alone might not fully impair this process in vivo. Importantly, in several models of skin diseases, PLA2G2F expression is increased in the thickened epidermis and its ablation attenuates epidermal hyperplasia in all of them. Thus, together with the findings that *Pla2g2f* is induced in keratinocytes by IL-22 and that *Pla2g2f*$^{tg/+}$ mice spontaneously develop psoriasis-like skin, it appears that aberrant PLA2G2F

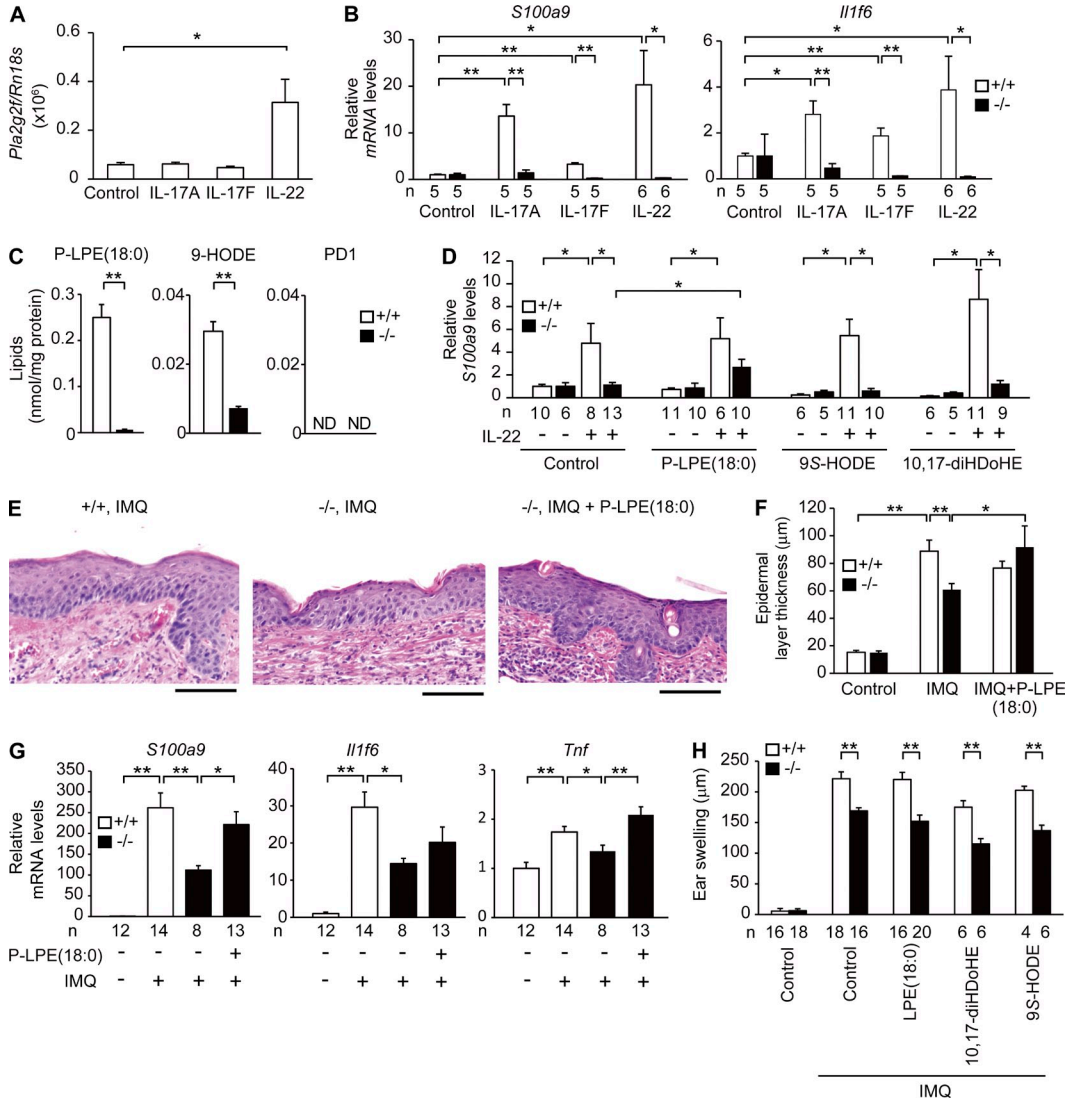

Figure 7. P-LPE rescues defective skin phenotypes in *Pla2g2f*$^{-/-}$ mice. (A and B) Quantitative RT-PCR of *Pla2g2f* (A) or *S100a9* and *Il1f6* (B) in keratinocytes after culture with or without Th17 cytokines (20 ng/ml) for 48 h ($n = 5$). (C) ESI-MS of lipid metabolites in culture medium of *Pla2g2f*$^{+/+}$ and *Pla2g2f*$^{-/-}$ keratinocytes after stimulation with IL-22 for 48 h ($n = 6$). (D) Quantitative RT-PCR of *S100a9* in *Pla2g2f*$^{+/+}$ and *Pla2g2f*$^{-/-}$ keratinocytes treated for 48 h with various lipids (10 nM) in the presence or absence of IL-22 ($n = 5$). (E) Hematoxylin-eosin staining of IMQ-treated *Pla2g2f*$^{+/+}$ and *Pla2g2f*$^{-/-}$ ears with or without P-LPE(18:0) at day 5 (bar, 100 µm). (F) Epidermal thickness of *Pla2g2f*$^{+/+}$ and *Pla2g2f*$^{-/-}$ ears treated with or without (control) IMQ or P-LPE(18:0) for 5 d ($n = 8$). (G) Quantitative RT-PCR of *Pla2g2f*$^{+/+}$ and *Pla2g2f*$^{-/-}$ ears treated with or without IMQ or P-LPE(18:0) for 5 d. (H) Effects of various lipids on IMQ-induced ear swelling in *Pla2g2f*$^{+/+}$ and *Pla2g2f*$^{-/-}$ mice at day 5. In B, D, and G, expression was normalized with *Rn18s* or *Gapdh*, the values for the control WT group being 1. Data are representative of two (A–C and E) or three (D) experiments, or are compiled from two experiments (F–H; mean ± SEM; *, $P < 0.05$; **, $P < 0.01$). ND, not detected.

expression, itself, can trigger keratinocyte hyperplasia and activation. Persistent abnormalities in keratinocyte activation and barrier function by the absence of PLA2G2F may stimulate downstream inflammation by secondary mechanisms (e.g., inflammatory cytokine production).

In one scenario, free fatty acids in the SC interfaces may be generated by sPLA$_2$-catalyzed release from bulk phospholipids secreted from keratinocytes (Mao-Qiang et al., 1996; Fluhr et al., 2001, 2004; Ilic et al., 2014; Man et al., 2014). Our results, although partially supportive of this idea, rather fit with the view that particular lipid metabolites driven by a given sPLA$_2$ influence keratinocyte functions, thereby affecting epidermal pathophysiology. We found that PLA2G2F preferentially cleaves a specific class of phospholipid, P-PE (plasmalogen), secreted from keratinocytes to yield P-LPE (lysoplasmalogen) and DHA, rather than hydrolyzing all phospholipid species nonselectively as has been previously thought. Moreover, the levels of its hydrolytic products, particularly P-LPE, are associated with those of *Pla2g2f* expression in distinct models. Thus, in line with our previous studies

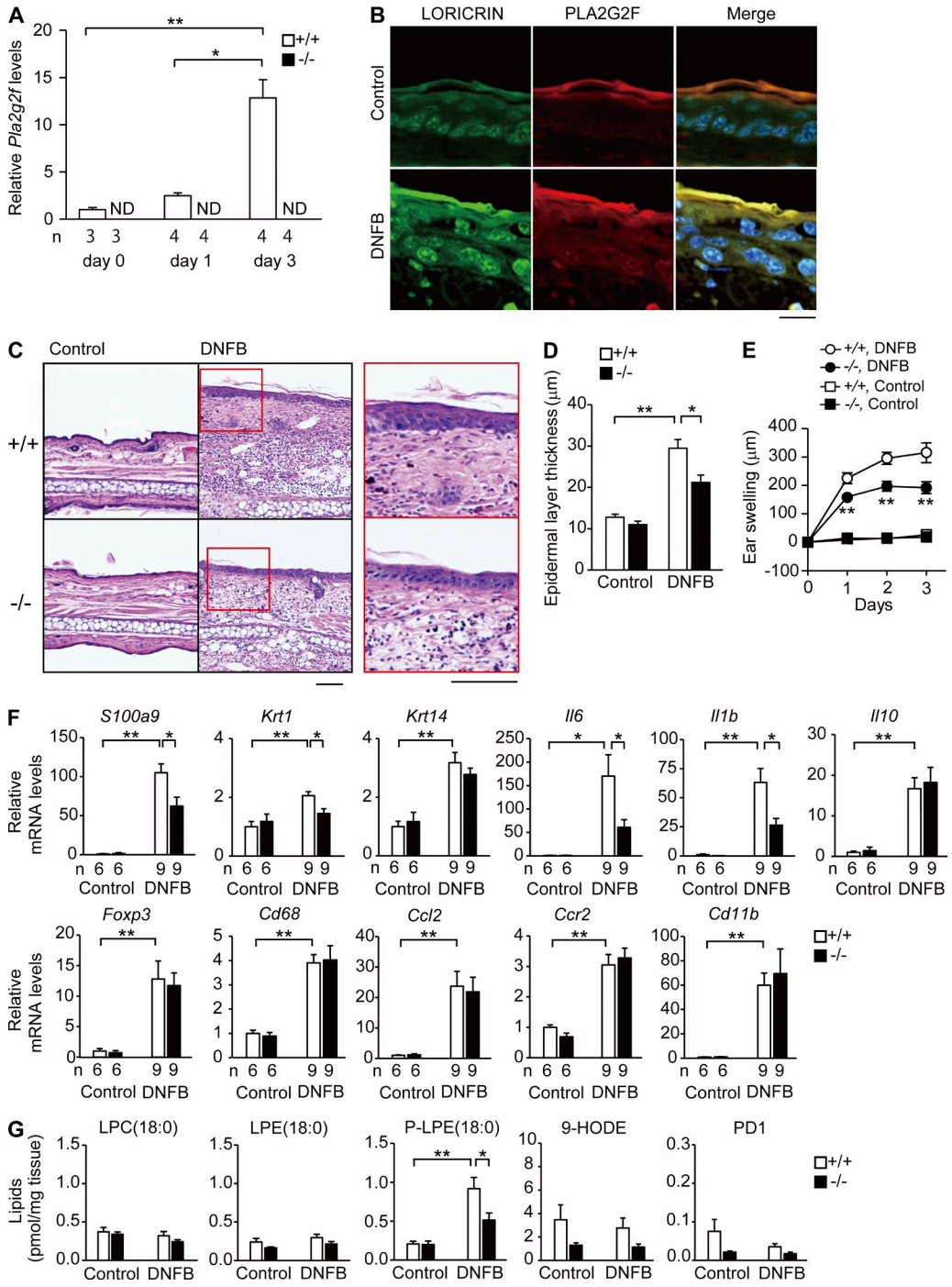

Figure 8. Reduced contact dermatitis in *Pla2g2f*$^{-/-}$ mice. (A) Quantitative RT-PCR of *Pla2g2f* in *Pla2g2f*$^{+/+}$ and *Pla2g2f*$^{-/-}$ ears after treatment with DNFB. (B) Confocal microscopy of PLA2G2F (red), loricrin (green), and their merged images (yellow) in WT skin on day 3, with DAPI counterstaining (blue; bar, 20 µm). (C) Hematoxylin-eosin staining of *Pla2g2f*$^{+/+}$ and *Pla2g2f*$^{-/-}$ skins on day 3 (bar, 50 µm). Boxes are magnified in right panels. (D and E) Epidermal thickness ($n = 6$; D) or time-dependent ear swelling ($n = 8$; E) of *Pla2g2f*$^{+/+}$ and *Pla2g2f*$^{-/-}$ mice on day 3. (F) Quantitative RT-PCR of keratinocyte or immune cell markers in *Pla2g2f*$^{+/+}$ and *Pla2g2f*$^{-/-}$ ears on day 3 ($n = 6$). (G) ESI-MS of lipid metabolites in *Pla2g2f*$^{+/+}$ and *Pla2g2f*$^{-/-}$ ears on day 3 ($n = 6$). In A and F, expression was normalized with *Gapdh*, the values for the control WT group being 1. Data are compiled from two experiments (D–F) or are representative of two experiments (A and G; mean ± SEM; *, $P < 0.05$; **, $P < 0.01$). Images are representative of two experiments (B and C). ND, not detected.

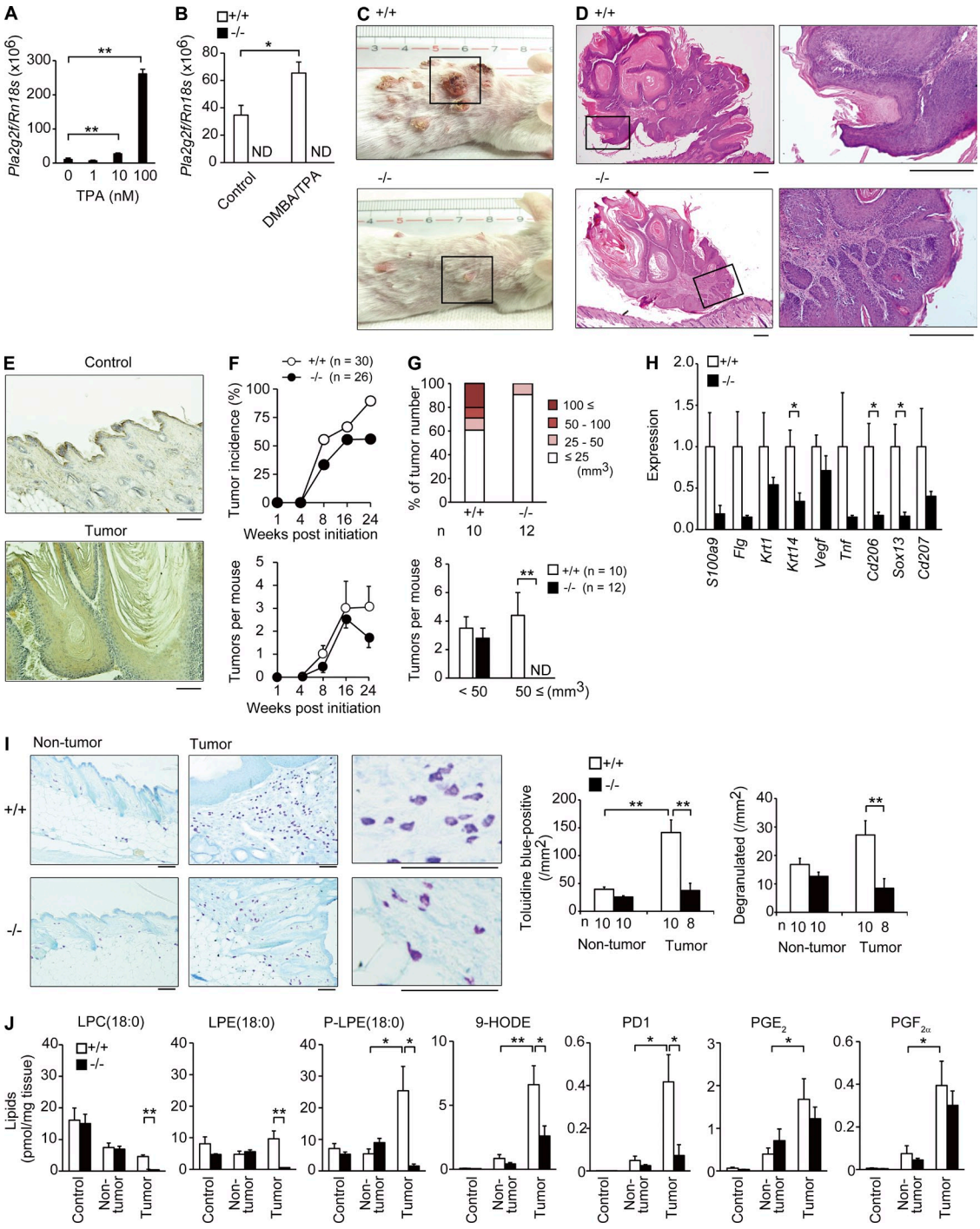

Figure 9. Reduced skin carcinogenesis in *Pla2g2f*$^{-/-}$ mice. (A and B) Quantitative RT-PCR of *Pla2g2f* in WT keratinocytes 48 h after treatment with TPA ($n = 6$; A) or in *Pla2g2f*$^{+/+}$ and *Pla2g2f*$^{-/-}$ skins (BALB/c background) 4 wk after treatment with or without DMBA/TPA ($n = 6$; B). (C and D) Gross appearances of *Pla2g2f*$^{+/+}$ and *Pla2g2f*$^{-/-}$ mice (C) and hematoxylin-eosin staining of skin tumors (D) at 24 wk (bar, 100 µm). Boxes are magnified in the right panels (D). (E) Immunohistochemistry of PLA2G2F in tumor and nontumor areas of DMBA/TPA-treated WT skin at 24 wk. (F and G) Monitoring of tumor incidence, numbers (F), and sizes (G) in DMBA/TPA-treated *Pla2g2f*$^{+/+}$ and *Pla2g2f*$^{-/-}$ skins ($n = 9$). (H) Quantitative RT-PCR of keratinocyte or immune cell genes in DMBA/TPA-treated *Pla2g2f*$^{+/+}$ and *Pla2g2f*$^{-/-}$ skins at 24 wk, the expression levels in WT being 1 ($n = 6$). (I) Toluidine blue staining of skin mast cells at 24 wk. Right panels show magnified views, in which degranulated mast cells were frequently seen in *Pla2g2f*$^{+/+}$, but not in *Pla2g2f*$^{-/-}$, mice. Total and degranulated mast cells were counted (bar, 100 µm). (J) ESI-MS of lipid metabolites in *Pla2g2f*$^{+/+}$ and *Pla2g2f*$^{-/-}$ skins 24 wk after treatment with (nontumor and tumor) or without (control) DMBA/TPA ($n = 6$). Data are compiled from two (B) or three experiments (F–H and J) or from one (A) or two (I) experiments (mean ± SEM; *, $P < 0.05$; **, $P < 0.01$). Representative images are shown (C–E and I). ND, not detected.

(Miki et al., 2013; Sato et al., 2014), several $sPLA_2$s act selectively on particular phospholipids to generate specific products other than canonical AA metabolites, which may underlie their distinct functions.

Although little is known about the biological activity of P-LPE, we show here that it can rescue the hyperproliferation and activation defects of *Pla2g2f*$^{-/-}$ keratinocytes both ex vivo and in vivo. We therefore speculate that P-LPE itself, or after conversion to other lipid metabolites, may behave like a lipid mediator that regulates skin inflammation and cancer, as well as barrier homeostasis. It is also possible that PLA2G2F may affect skin pathophysiologies through mobilization of some other unidentified lipid products, whose molecular identity awaits future studies. Nonetheless, our results have revealed P-LPE to be a novel biomarker and driver of skin diseases in which PLA2G2F is involved.

Hydrolysis of P-LPE by PLA2G2F gives rise to DHA and its metabolite PD1 in the skin in several if not all models. Because our MS analysis did not precisely discriminate PD1 (10*R*,17*S*-diHDoHE) and its stereoisomer (10*S*,17*S*-diHDoHE or protectin DX), the possibility that we measured the mixture of PD1 and 10*S*,17*S*-diHDoHE cannot be ruled out, although the latter is not the major product of human cells (Serhan et al., 2000; Hong et al., 2003). PD1 and its isomer have been shown to stop neutrophil recruitment, reduce inflammation, and stimulate resolution (Serhan, 2014; Serhan et al., 2015). Although PD1 or its isomer may not be involved in psoriatic epidermal hyperplasia, PD1 formation in the skin as discovered in the present work may be relevant in limiting acute inflammation and stimulating resolution of skin inflammation and the return to homeostasis. In this regard, our result showing an increase in Ca^{2+}-induced *Krt1* expression by the PD1 isomer may reflect its role in adequate keratinocyte differentiation and barrier homeostasis.

As LA is crucial for skin homeostasis (Elias et al., 2014), some of the phenotypes observed in *Pla2g2f*$^{-/-}$ mice may be based on the disturbed LA metabolism. Indeed, one of the PLA2G2F-driven lipid products, 9*S*-HODE, increased Ca^{2+}-dependent, but not IL-22–induced, *S100a9* expression in keratinocytes, underscoring the key and distinct roles of this LA metabolite in PLA2G2F-regulated epidermal biology. However, given the substrate selectivity of PLA2G2F, the PLA2G2F-dependent changes in LA metabolism may largely or even solely reflect an indirect consequence of altered keratinocyte differentiation or activation. From this viewpoint, other PLA_2s or lipases may be responsible for the supply of a large pool of LA in association with keratinocyte differentiation. Candidate genes for this process include *ABHD5*, *PNPLA1*, and *LIPN*, which belong to the lipase family, are expressed in keratinocytes, and cause ichthyosis when mutated (Akiyama et al., 2003; Israeli et al., 2011; Grall et al., 2012).

Current therapies for psoriasis involve biologics that target cytokines, such as TNF, IL-17, or IL-23, and their efficacy has been proven in clinical trials (Lowes et al., 2014). However, inhibition of these cytokines may render individuals susceptible to infection due to undesirable immune defects, underlining the need for tissue-specific targets. Nonsurgical management for skin cancer includes the use of chemotherapy, in which currently used agents may have survival benefits but also undesirable adverse effects. Given that PLA2G2F is expressed in the epidermis rather specifically, blocking PLA2G2F may be a novel approach for specific treatment of psoriasis, skin cancer, or other conditions characterized by epidermal hyperplasia.

MATERIALS AND METHODS

Mice. All mice were housed in climate-controlled (23°C) specific pathogen–free facilities with a 12-h light/dark cycle, with free access to standard laboratory food (CE2; Laboratory Diet; CLEA Japan) and water. Male mice were used in most studies. All procedures involving animals were performed in accordance with protocols approved by the Institutional Animal Care and Use Committees of the Tokyo Metropolitan Institute of Medical Science, Showa University, and the University of Washington.

Generation of *Pla2g2f*$^{tg/+}$ mice. The strategy for the generation of TG mice for $sPLA_2$s has been reported previously (Yamamoto et al., 2011b). In brief, the cDNA for mouse *Pla2g2f* was inserted into the EcoRI site (downstream of the *CAG* [cytomegalovirus immediate early enhancer-chicken β-actin hybrid] promoter) in the pCALNL5 vector (Kanegae et al., 1996; Fig. 2 A). The plasmid, containing the transgene downstream of a neomycin cassette (*Neo*^{r}) with *LoxP* sites at both ends, was excised at the HindIII and SalI sites to produce a 6-kb *CAG-LoxP-Neo*^{r}*-LoxP-Pla2g2f* (*LNL-Pla2g2f*) fragment. Then, the DNA was injected into fertilized eggs. Genotyping was performed on genomic DNA from tail biopsies by PCR using the primer pairs 5′-TGGTTATTGTGCTGTCTCATCATTT-3′ and 5′-CACCATGGACTTCAGGTTCAG-3′ (Sigma-Aldrich), which amplified a 1,600-bp fragment specific for *LNL-Pla2g2f*. The reaction was 95°C for 10 s, and then 35 cycles of 95°C for 0 s and 65°C for 1 min on an Applied Biosystems 9800 Fast Thermal Cycler (Applied Biosystems). The PCR products were analyzed by 1.5% (wt/vol) agarose gel electrophoresis with ethidium bromide. Male founders were mated with female C57BL/6 mice (Japan SLC) to confirm germ line transmission by PCR genotyping, and those with successful germ line transmission (*LNL-Pla2g2f*$^{tg/+}$) were then crossed with female *CAG-Cre*$^{tg/+}$ mice, which carry the Cre recombinase transgene under control of the *CAG* promoter (Kanegae et al., 1996). This step resulted in removal of the *Neo*^{r} cassette from the *LNL-Pla2g2f* transgene, thereby allowing activation of the *Pla2g2f* transgene in the whole body of the offspring (Fig. 2, A and B). All of the *Pla2g2f*$^{tg/+}$ mice were inbred with C57BL/6 mice. Phenotypes that appeared in *Pla2g2f*$^{tg/+}$ mice, which carried the active *Pla2g2f* transgene, but not in *LNL-Pla2g2f*$^{tg/+}$ mice, in which the *Pla2g2f* transgene remained silent, were regarded as events caused by the overexpressed PLA2G2F. For skin-specific TG overexpression, *LNL-Pla2g2f*$^{tg/+}$ mice were crossed with *K14-Cre*$^{tg/+}$ mice (Andl et al., 2004). *PLA2G10*$^{tg/+}$ mice were reported previously (Yamamoto et al., 2011b).

Gene targeting of *Pla2g2f*. The *Pla2g2f*-targeting vector was constructed with the *Neo*^{r} gene that was inserted between exons 1 and 2 of the *Pla2g2f* gene with *LoxP* sites at both ends (Fig. 3 A). ES cell transfection and embryo injections were performed by the Transgenic Resources Program (Department of Comparative Medicine, University of Washington). ES clones with homologous recombination were screened by PCR and Southern blotting. The founder heterozygous mice (129 x C57BL/6 background) with germ line transmission were crossed with *CAG-Cre*$^{tg/+}$ mice to delete exons 2 and 3 plus the *Neo*^{r} cassette in the offspring. Genotyping was performed on genomic DNA from tail biopsies by PCR using the primer pairs 5′-CAGTCAGCTGCCCTCTTTTAGAA-3′ and 5′-GTGGGTCATCCTGGGTTTGT-3′ (Sigma-Aldrich), which amplified a 490-bp fragment specific for the WT allele, and 5′-CATCCGGCTAAGGACAACAGA-3′ and 5′-GTGGGTCATCCTGGGTTTGT-3′, which amplified a 325-bp fragment specific for the mutant allele. *Pla2g2f*$^{+/-}$ mice were backcrossed to

C57BL/6 or BALB/c mice (Japan SLC) for more than 12 generations and then intercrossed to obtain *Pla2g2f*$^{-/-}$ and *Pla2g2f*$^{+/+}$ mice. This *Pla2g2f*$^{-/-}$ mouse line was used in a previous study (Ilic et al., 2014). Knockout mice for other sPLA$_2$s were described previously (Yamamoto et al., 2011b; Miki et al., 2013; Sato et al., 2014).

Histological examination. Histochemistry of mouse skin sections was performed as described previously (Yamamoto et al., 2011b). In brief, skin samples were fixed with 100 mM phosphate buffer (pH 7.2) containing 4% (wt/vol) paraformaldehyde, embedded in paraffin, sectioned, mounted on glass slides, deparaffinized in xylene, and rehydrated in ethanol with increasing concentrations of water. Hematoxylin and eosin staining was performed on the 5-µm-thick cryosections. Paraffin-embedded tissue sections were incubated with Target Retrieva Solution (Dako), and then with rabbit anti–mouse PLA2G2F antibody (Degousee et al., 2002), which did not cross-react with other sPLA$_2$s, or control antibody at 1:2,000 dilution in 10 mM Tris-HCl (pH 7.4) containing 0.15 M NaCl and 0.1% (wt/vol) BSA (TBS-BSA) overnight at 4°C. The sections were then treated with an EnVision+^{R} System Staining kit (Dako) with diaminobenzidine substrate, followed by counterstaining with hematoxylin. The stained sections were analyzed with a BX61 microscope (Olympus). Epidermal layer thickness was measured using DP2-BSW software (Olympus).

Immunofluoresence staining. 5-µm-thick mouse or human tissue sections were incubated with 1x Blockace (DS Pharma BioMedical) in PBS-T for 30 min, washed three times with PBS-T for 5 min each, and incubated with rabbit anti–mouse or –human PLA2G2F antibody (Degousee et al., 2002) at 1:500–1,000 dilution in a 10-fold-diluted Blockace for overnight at 4°C. The sections were then washed 3 times with PBS-T for 5 min each time and incubated with Alexa Fluor 647–labeled goat anti–rabbit IgG antibody (Molecular Probes; 1:1,000) at 20°C for 1 h. For double immunostaining, the sections were washed three times with PBS-T for 5 min each and incubated with rabbit antibodies against mouse loricrin, cytokeratin 1 and cytokeratin 5 (PRB-145P, PRB-165P and PRB-160P [Covance], respectively; 1:500) prelabeled with Alexa Fluor 555 (Zenon Labeling System; Molecular Probes) at 20°C for 1 h. Counterstaining was performed with 4,6-diamino-2-phenylindole (DAPI; Vector Laboratories). Stained sections were analyzed with a confocal laser-scanning microscope (LSM510 META, Carl Zeiss). Human skin sections were obtained by surgery at Chiba University (Chiba, Japan) after approval by the Faculty ethics committee and informed consents from patients.

Immunoblotting. The dorsal and abdominal skins of 10-mo-old mice were washed with 10 ml/mouse of a urea buffer comprising 5 M urea, 2 M thiourea, and 1 mM EDTA in PBS supplemented with a protease inhibitor cocktail (Roche). The washed skins were scrapped with the edge of a slide glass and continuously rinsed with 8 M urea solution. The buffer containing corneocytes was collected in a container placed below the mice. Corneocytes were removed by centrifugation at 3,000 *g* for 30 min at 4°C. The supernatants were concentrated using an Amicon-ultra 10K (EMD Millipore). Protein concentrations were determined with a BCA protein assay kit (Thermo Fisher Scientific). The extracts (50-µg protein equivalents) were subjected to NuPAGE-PAGE on 4–12% (wt/vol) gels (Life Technologies) under reducing conditions and then electroblotted onto PVDF membranes (Bio-Rad Laboratories) with a semi-dry blotter (Transblot SD; Bio-Rad Laboratories). The membranes were blocked with 5% (wt/vol) skim milk in PBS containing 0.05% (vol/vol) Tween-20 (PBS-T), probed with rabbit anti-mouse PLA2G2F antibody (1:1,000) in PBS-T for 2 h, incubated with horseradish peroxidase–conjugated anti–rabbit IgG (Invitrogen) at 1:5,000 dilution in PBS-T for 2 h, and then visualized using ECL Prime Western blotting detection reagent (GE Healthcare Life Science) with LAS-4000 (Fuji Film).

Corneocyte stability. The SC samples were prepared by boiling of the epidermis for 30 min in a buffer consisting of 20 mM Tris-HCl, pH 7.5, 5 mM EDTA, 10 mM dithiothreitol (DTT), and 2% SDS. After centrifugation at 5,000 *g*, isolated corneocytes were washed twice at room temperature with a buffer consisting of 20 mM Tris-HCl, pH 7.5, 5 mM EDTA, 10 mM DTT, and 0.2% SDS. The corneocytes were suspended in 2% SDS solution and counted. The corneocyte suspensions were sonicated by a ultrasonic sonicator (EYEL4; Tokyo Rikakikai) for various time periods, and aliquots were taken for microscopic analyses.

In situ hybridization. *Pla2g2f* cDNA was subcloned into the pGEMT-Easy vector (Promega), and used for generation of sense or anti-sense RNA probes. Digoxigenin labeled-RNA probes were prepared with DIG RNA labeling Mix (Roche). 6-µm-thick paraffin-embedded sections of mouse skin were hybridized with the digoxigenin-labeled RNA probes at 60°C for 16 h (Genostaff). The bound label was detected using the alkaline phosphate color substrates nitro-blue tetrazolium chloride and 5-bromo-4-chloro-3′-indolylphosphatase *p*-toluidine salt. The sections were counterstained with Kernechtrot (Muto Pure Chemicals).

Transmission electron microscopy. Tissues were fixed with 100 mM phosphate buffer (pH 7.2) containing 1% (vol/vol) glutaraldehyde and 4% (wt/vol) paraformaldehyde, post-fixed with 2% (wt/vol) OsO_4 in PBS, dehydrated through a graded ethanol series, passed through propylene oxide, and embedded in Poly/Bed 812 EPON (Polyscience). 0.08-µm-thick ultrathin sections were stained with uranyl acetate and lead citrate, and then examined using an electron microscope (H-7600; Hitachi).

Quantitative RT-PCR. Total RNA was extracted from tissues and cells using TRIzol reagent (Invitrogen). First-strand cDNA synthesis was performed using a High Capacity cDNA Reverse transcription kit (Applied Biosystems). PCR reactions were performed using a Power SYBR Green PCR system (Applied Biosystems) or a TaqMan Gene Expression System (Applied Biosystems) on the ABI7300 Quantitative PCR system (Applied Biosystems). The probe/primer sets used are listed in Table S4.

Microarray analysis. Total RNA extracted from skins or keratinocytes were purified using the RNeasy Mini kit (QIAGEN). The quality of RNA was assessed with a 2100 Bioanalyzer (Agilent Technologies). cRNA targets were synthesized and hybridized with Whole Mouse Genome Microarray according to the manufacturer's instructions (G4122A or G4846A; Agilent Technologies). The array slides were scanned using a Laser Scanner GenePix 4000B (Molecular Devices) or a SureScan Microarray Scanner (Agilent Technologies). Microarray data were analyzed with GenePix Software (Molecular Devices) or Agilent's Feature Extraction Software. The Gene Expression Omnibus accession nos. for microarrays (Tables S1, S2, and S3) are GSE71827, GSE71829, and GSE71826, respectively.

Lipid metabolome. Samples for ESI-MS of phospholipids/ceramides and fatty acid derivatives were prepared separately and analyzed as described previously (Miki et al., 2013;Yamamoto et al., 2011b). In brief, for detection of phospholipids and ceramides, tissues were soaked in 10 volumes of 20 mM Tris-HCl (pH 7.4) and then homogenized with a Polytron homogenizer. Lipids were extracted from the homogenates by the method of Bligh and Dyer (Bligh and Dyer, 1959). As an internal standard for determination of recovery, 1 nmol LPC (17:0; Avanti) was added to each sample. The analysis was performed using a 4000Q-TRAP quadrupole-linear ion trap hybrid mass spectrometer (AB Sciex) with liquid chromatography (LC; NexeraX2 system; Shimazu). The sample was applied to a Develosil C30-UG column (1 × 150 mm i.d., 3-µm particle; Nomura Chemical) coupled for ESI-MS/MS. The samples injected by an autosampler (10 µl) were separated by a step gradient with mobile phase A (acetonitrile/methanol/water = 1:1:1 [vol/vol/vol] containing 5 µM phosphoric acid and 1 mM ammonium formate) and mobile phase B (2-propanol containing 5 µM phosphoric acid and 1 mM ammonium formate) at a flow rate of 80 µl/min at 50°C. Identification was conducted using multiple reaction monitoring (MRM) transition and retention times, and quantification was performed based on peak area of the

MRM transition and the calibration curve obtained with an authentic standard for each compound (Table S5).

For detection of fatty acids and their oxygenated metabolites, tissues were soaked in 10 volumes of methanol and then homogenized with a Polytron homogenizer. After overnight incubation at −20°C, water was added to the mixture to give a final methanol concentration of 10% (vol/vol). As an internal standard, 1 nmol of *d5*-labeled EPA and *d4*-labeled PGE_2 (Cayman Chemicals) was added to each sample. The samples in 10% methanol were applied to Sep-Pak C18 cartridges (Waters), washed with 10 ml of hexane, eluted with 3 ml of methyl formate, dried up under N_2 gas, and dissolved in 60% methanol. The samples were then applied to a Develosil C30-UG column (1 × 150 mm i.d., 3-µm particles; Nomura Chemical) coupled for ESI-MS/MS as described above. The samples injected by an autosampler (10 µl) were separated using a step gradient with mobile phase C (water containing 0.1% acetic acid) and mobile phase D (acetonitrile/methanol = 4:1; vol/vol) at a flow rate of 50 µl/min at 45°C. Chiral HPLC analysis was performed using a Chiralpak IA-3 column (4.6 × 150 mm i.d., 3-µm particles; Daicel) with mobile phase E (acetonitrile/methanol/H_2O = 68:17:15 [vol/vol/vol] containing 0.1% acetic acid) at a flow rate of 0.2 ml/min at 25°C. Each lipid was detected and quantified as described above.

Keratinocyte culture. Keratinocytes were isolated from the whole skin of newborn mice using 0.05% (wt/vol) collagenase A (Roche) in KGM (−) medium (MCDB 153 medium [Sigma-Aldrich] supplemented with 0.5 µg/ml hydrocortisone, 14.1 µg/ml phosphorylethanolamine, 0.2% [vol/vol] Matrigel [BD], 100 U/ml penicillin, and 100 mg/ml streptomycin) overnight at 4°C. Then, the cells were cultured with KGM (+) medium (KGM [−] medium supplemented with 5 ng/ml insulin, 10 ng/ml EGF, and 40 µg/ml bovine pituitary extract]. After 3 d, the cells were treated with 1 mM $CaCl_2$ or the Th17 cytokines IL-17A, IL-17F or IL-22 (20 ng/ml; ProSpec) in KGM (+) medium. After appropriate periods, RNA was extracted from the cells and subjected to quantitative RT-PCR, and the supernatants were subjected to PLA_2 assay and lipid metabolome. As required for experiments, the $sPLA_2$ inhibitor LY315920 (2-(3-(2-amino-2-oxoacetyl)-1-benzyl-2-ethyl-1*H*-6,7-benzoindol-4-yloxy)acetic acid) or its placebo (2-(3-(2-N-methylamino-2-oxoacetyl)-1-benzyl-2-ethyl-1*H*-6,7- benzoindol-4-yloxy) acetic acid; Oslund et al., 2008), recombinant mouse PLA2G2F (Valentin et al., 1999; Singer et al., 2002), fatty acid derivatives (9*S*-HODE or 10,17-DiHDoHE; Cayman Chemical), and LPE species (LPE(18:0) or P-LPE(18:0); Avanti) were added to the culture.

Newborn human epidermal keratinocytes (NHEK; Kurabo) were cultured in HuMedia KG2 Medium (Kurabo) for 1 d. NHEK cells were transfected with 10 nM human *PLA2G2F* siRNA (Flexi Tube siRNA, Hs_PLA2G2F_2; 5′-TACCAGGAACTCTTTGACCAA-3′; QIAGEN) or control siRNA (All Stars Negative Control siRNA; QIAGEN) using Lipofectamine RNAiMAX (Invitrogen), in accordance with the manufacturer's instructions. After 3 d, the medium was changed to Assay Medium (Japan Tissue Engineering) for cell differentiation. After 2 d, RNA was extracted from the cells and subjected to quantitative RT-PCR.

IMQ-induced psoriasis. Mice (BALB/c background; 8–12-wk-old males) received a daily topical application of 12.5 µg of 5% IMQ or vehicle cream (Mochida Pharma) on the dorsal and ventral surfaces of the ears over 4 d (total 50 µg of IMQ cream per mouse). As required for the experiments, 10 nM lipids were topically applied to the ears every day. Ear thickness was monitored at various time points with a micrometer. On day 6, the mice were sacrificed and subjected to quantitative RT-PCR, histochemistry and lipid metabolome analysis.

Hapten-induced contact dermatitis. On day −5, mice (C57BL/6 background; 8–12-wk-old, males) were sensitized with 50 µl of 0.5% (wt/vol) DNFB in acetone/olive oil (4/1; vol/vol) on the shaved abdominal skin. On day 0, the dorsal and ventral surfaces of the ears were challenged with 20 µl of 0.3% DNFB. Ear thickness was monitored at various time points with a micrometer. On day 3, the mice were sacrificed and subjected to quantitative RT-PCR, histochemistry, and lipidomics analysis.

DMBA/TPA-induced skin carcinogenesis. The back skin of mice (BALB/c background, 8-wk-old, female) was shaved with an electric clipper. 1 wk later, 200 µl of 2 mM DMBA (Sigma-Aldrich) in acetone was applied to the shaved skin. After 1 wk, 200 µl of 80 µM TPA (Sigma-Aldrich) in acetone was applied to the skin twice a week over 24 wk. Cutaneous papillomas were counted and scored weekly. The mice were then sacrificed and subjected to quantitative RT-PCR, histochemistry, and lipidomics analysis.

Flow cytometry. Mouse ear skin was incubated in 0.25% (wt/vol) trypsin/EDTA solution (Sigma-Aldrich) for 1 h at 37°C for separation of the epidermis from the dermis. RPMI-1640 medium (Sigma-Aldrich) containing 1.6 mg/ml collagenase IV (Worthington) was used to obtain dermal cell suspensions, which were passed through a Cell Strainer 70-µm Nylon (Falcon; BD) and then centrifuged at 300 *g* for 5 min at 4°C. For surface staining, the cells were blocked with mouse BD Tc Block and incubated with various cell surface marker antibodies (listed in Table S6). For intracellular staining, the cells that had been stained with surface marker antibodies were fixed, permeabilized with 1 µg/ml ionomycin, 25 ng/ml phorbol ester, and 0.5 µl/ml GolgiStop (BD) for 4 h, and then stained with anti-cytokine antibodies (listed in Table S5). Flow cytometry was performed with a FACSAria III (BD) and FlowJo (Tree Star) software.

Other procedures. TEWL of mouse skin was determined using a Tewameter TM300 (Courage and Khazaka). Cutaneous pH was measured with a flat, glass surface electrode (Skin-pH-MeterPH 905; Courage and Khazaka). Serum biochemical markers were analyzed using the clinical chemistry analyzer VetScan with V-DPP rotors (Abaxis). Laser-capture microdissection of the epidermis and hair follicles from mouse skin and Northern blotting were performed as described previously (Yamamoto et al., 2011b).

Statistical analyses. All values are given as the mean ± SEM. Differences between two groups were assessed by unpaired Student's *t*-test using the Excel Statistical Program File ystat 2008 (Igaku Tosho Shuppan). Differences at p-values of <0.05 were considered statistically significant.

Online supplemental material. Table S1 shows microarray gene profiling of lipase-related genes in *PLA2G10*$^{tg/+}$ and WT skins. Table S2 shows microarray gene profiling of *Pla2g2f*$^{tg/+}$ and WT skins. Table S3 shows microarray gene profiling of *Pla2g2f*$^{+/+}$ and *Pla2g2f*$^{-/-}$ keratinocytes. Table S4 is a list of primers for quantitative RT-PCR. Table S5 indicates MRM transitions for the identification of lipids. Table S6 is a list of antibodies for flow cytometry. Online supplemental material is available at http://www.jem.org/cgi/content/full/jem.20141904/DC1.

We thank Dr. A. Brash (Vanderbilt University, Nashville, TN) for helpful discussion and Drs. S. Arata and A. Ohazama (Showa University, Tokyo, Japan) for providing *Cre-CAG or -K14* TG mice.

This work was supported by grants-in aid for Scientific Research fro the Ministry of Education, Culture, Sports, Science and Technology of Japan 22116005, 24390021, and 15H05905 (to M. Murakami), 23591665, 26461671 (to K. Yamamoto) and 26860051 (to Y. Miki), the JSPS-National Science Foundation Bilateral Joint Project FY2012 (to M. Murakami), Core Research for Evolutional Science and Technology from the Agency for Medical Research and Development (to M. Murakami), the Uehara, Mitsubishi, Terumo and Toray Science Foundations (to M. Murakami), and National Institutes of Health grant HL36235 (to M.H. Gelb).

The authors declare no competing financial interests.

Submitted: 5 October 2014
Accepted: 31 August 2015

REFERENCES

Ait-Oufella, H., O. Herbin, C. Lahoute, C. Coatrieux, X. Loyer, J. Joffre, L. Laurans, B. Ramkhelawon, O. Blanc-Brude, S. Karabina, et al. 2013. Group X secreted phospholipase A_2 limits the development of atherosclerosis in LDL receptor-null mice. *Arterioscler. Thromb. Vasc. Biol.* 33:466–473. http://dx.doi.org/10.1161/ATVBAHA.112.300309

Akiyama, M., D. Sawamura, Y. Nomura, M. Sugawara, and H. Shimizu. 2003. Truncation of CGI-58 protein causes malformation of lamellar granules resulting in ichthyosis in Dorfman-Chanarin syndrome. *J. Invest. Dermatol.* 121:1029–1034. http://dx.doi.org/10.1046/j.1523-1747.2003.12520.x

Andl, T., K. Ahn, A. Kairo, E.Y. Chu, L. Wine-Lee, S.T. Reddy, N.J. Croft, J.A. Cebra-Thomas, D. Metzger, P. Chambon, et al. 2004. Epithelial Bmpr1a regulates differentiation and proliferation in postnatal hair follicles and is essential for tooth development. *Development.* 131:2257–2268. http://dx.doi.org/10.1242/dev.01125

Bazan, N.G., J.M. Calandria, and C.N. Serhan. 2010. Rescue and repair during photoreceptor cell renewal mediated by docosahexaenoic acid-derived neuroprotectin D1. *J. Lipid Res.* 51:2018–2031. http://dx.doi.org/10.1194/jlr.R001131

Bligh, E.G., and W.J. Dyer. 1959. A rapid method of total lipid extraction and purification. *Can. J. Biochem. Physiol.* 37:911–917. http://dx.doi.org/10.1139/o59-099

Boudreau, L.H., A.C. Duchez, N. Cloutier, D. Soulet, N. Martin, J. Bollinger, A. Paré, M. Rousseau, G.S. Naika, T. Lévesque, et al. 2014. Platelets release mitochondria serving as substrate for bactericidal group IIA-secreted phospholipase A_2 to promote inflammation. *Blood.* 124:2173–2183. http://dx.doi.org/10.1182/blood-2014-05-573543

Condeelis, J., and J.W. Pollard. 2006. Macrophages: obligate partners for tumor cell migration, invasion, and metastasis. *Cell.* 124:263–266. http://dx.doi.org/10.1016/j.cell.2006.01.007

Degousee, N., F. Ghomashchi, E. Stefanski, A. Singer, B.P. Smart, N. Borregaard, R. Reithmeier, T.F. Lindsay, C. Lichtenberger, W. Reinisch, et al. 2002. Groups IV, V, and X phospholipases A_2s in human neutrophils: role in eicosanoid production and gram-negative bacterial phospholipid hydrolysis. *J. Biol. Chem.* 277:5061–5073. http://dx.doi.org/10.1074/jbc.M109083200

Elias, P.M., M.L. Williams, W.M. Holleran, Y.J. Jiang, and M. Schmuth. 2008. Pathogenesis of permeability barrier abnormalities in the ichthyoses: inherited disorders of lipid metabolism. *J. Lipid Res.* 49:697–714. http://dx.doi.org/10.1194/jlr.R800002-JLR200

Elias, P.M., R. Gruber, D. Crumrine, G. Menon, M.L. Williams, J.S. Wakefield, W.M. Holleran, and Y. Uchida. 2014. Formation and functions of the corneocyte lipid envelope (CLE). *Biochim. Biophys. Acta.* 314-318. 10.1016/j.bbalip.2013.09.011

Escoffier, J., I. Jemel, A. Tanemoto, Y. Taketomi, C. Payre, C. Coatrieux, H. Sato, K. Yamamoto, S. Masuda, K. Pernet-Gallay, et al. 2010. Group X phospholipase A_2 is released during sperm acrosome reaction and controls fertility outcome in mice. *J. Clin. Invest.* 120:1415–1428. http://dx.doi.org/10.1172/JCI40494

Fluhr, J.W., J. Kao, M. Jain, S.K. Ahn, K.R. Feingold, and P.M. Elias. 2001. Generation of free fatty acids from phospholipids regulates stratum corneum acidification and integrity. *J. Invest. Dermatol.* 117:44–51. http://dx.doi.org/10.1046/j.0022-202x.2001.01399.x

Fluhr, J.W., M. Mao-Qiang, B.E. Brown, J.P. Hachem, D.G. Moskowitz, M. Demerjian, M. Haftek, G. Serre, D. Crumrine, T.M. Mauro, et al. 2004. Functional consequences of a neutral pH in neonatal rat stratum corneum. *J. Invest. Dermatol.* 123:140–151. http://dx.doi.org/10.1111/j.0022-202X.2004.22726.x

Gareus, R., M. Huth, B. Breiden, A. Nenci, N. Rösch, I. Haase, W. Bloch, K. Sandhoff, and M. Pasparakis. 2007. Normal epidermal differentiation but impaired skin-barrier formation upon keratinocyte-restricted IKK1 ablation. *Nat. Cell Biol.* 9:461–469. http://dx.doi.org/10.1038/ncb1560

Grall, A., E. Guaguère, S. Planchais, S. Grond, E. Bourrat, I. Hausser, C. Hitte, M. Le Gallo, C. Derbois, G.J. Kim, et al. 2012. PNPLA1 mutations cause autosomal recessive congenital ichthyosis in golden retriever dogs and humans. *Nat. Genet.* 44:140–147. http://dx.doi.org/10.1038/ng.1056

Grass, D.S., R.H. Felkner, M.Y. Chiang, R.E. Wallace, T.J. Nevalainen, C.F. Bennett, and M.E. Swanson. 1996. Expression of human group II PLA_2 in transgenic mice results in epidermal hyperplasia in the absence of inflammatory infiltrate. *J. Clin. Invest.* 97:2233–2241. http://dx.doi.org/10.1172/JCI118664

Hachem, J.P., M.Q. Man, D. Crumrine, Y. Uchida, B.E. Brown, V. Rogiers, D. Roseeuw, K.R. Feingold, and P.M. Elias. 2005. Sustained serine proteases activity by prolonged increase in pH leads to degradation of lipid processing enzymes and profound alterations of barrier function and stratum corneum integrity. *J. Invest. Dermatol.* 125:510–520. http://dx.doi.org/10.1111/j.0022-202X.2005.23838.x

Hattori, T., H. Obinata, A. Ogawa, M. Kishi, K. Tatei, O. Ishikawa, and T. Izumi. 2008. G2A plays proinflammatory roles in human keratinocytes under oxidative stress as a receptor for 9-hydroxyoctadecadienoic acid. *J. Invest. Dermatol.* 128:1123–1133. http://dx.doi.org/10.1038/sj.jid.5701172

Henderson, W.R. Jr., E.Y. Chi, J.G. Bollinger, Y.T. Tien, X. Ye, L. Castelli, Y.P. Rubtsov, A.G. Singer, G.K. Chiang, T. Nevalainen, et al. 2007. Importance of group X-secreted phospholipase A_2 in allergen-induced airway inflammation and remodeling in a mouse asthma model. *J. Exp. Med.* 204:865–877. http://dx.doi.org/10.1084/jem.20070029

Hong, S., K. Gronert, P.R. Devchand, R.L. Moussignac, and C.N. Serhan. 2003. Novel docosatrienes and 17S-resolvins generated from docosahexaenoic acid in murine brain, human blood, and glial cells. Autacoids in anti-inflammation. *J. Biol. Chem.* 278:14677–14687. http://dx.doi.org/10.1074/jbc.M300218200

Ilic, D., J.M. Bollinger, M. Gelb, and T.M. Mauro. 2014. $sPLA_2$ and the epidermal barrier. *Biochim. Biophys. Acta.* 1841:416–421. http://dx.doi.org/10.1016/j.bbalip.2013.11.002

Inoue, A., N. Arima, J. Ishiguro, G.D. Prestwich, H. Arai, and J. Aoki. 2011. LPA-producing enzyme PA-$PLA_1\alpha$ regulates hair follicle development by modulating EGFR signalling. *EMBO J.* 30:4248–4260. http://dx.doi.org/10.1038/emboj.2011.296

Israeli, S., Z. Khamaysi, D. Fuchs-Telem, J. Nousbeck, R. Bergman, O. Sarig, and E. Sprecher. 2011. A mutation in LIPN, encoding epidermal lipase N, causes a late-onset form of autosomal-recessive congenital ichthyosis. *Am. J. Hum. Genet.* 88:482–487. http://dx.doi.org/10.1016/j.ajhg.2011.02.011

Jobard, F., C. Lefèvre, A. Karaduman, C. Blanchet-Bardon, S. Emre, J. Weissenbach, M. Ozgüc, M. Lathrop, J.F. Prud'homme, and J. Fischer. 2002. Lipoxygenase-3 (ALOXE3) and 12(R)-lipoxygenase (ALOX12B) are mutated in non-bullous congenital ichthyosiform erythroderma (NCIE) linked to chromosome 17p13.1. *Hum. Mol. Genet.* 11:107–113. http://dx.doi.org/10.1093/hmg/11.1.107

Kanegae, Y., K. Takamori, Y. Sato, G. Lee, M. Nakai, and I. Saito. 1996. Efficient gene activation system on mammalian cell chromosomes using recombinant adenovirus producing Cre recombinase. *Gene.* 181:207–212. http://dx.doi.org/10.1016/S0378-1119(96)00516-1

Koch, P.J., P.A. de Viragh, E. Scharer, D. Bundman, M.A. Longley, J. Bickenbach, Y. Kawachi, Y. Suga, Z. Zhou, M. Huber, et al. 2000. Lessons from loricrin-deficient mice: compensatory mechanisms maintaining skin barrier function in the absence of a major cornified envelope protein. *J. Cell Biol.* 151:389–400. http://dx.doi.org/10.1083/jcb.151.2.389

Labonté, E.D., R.J. Kirby, N.M. Schildmeyer, A.M. Cannon, K.W. Huggins, and D.Y. Hui. 2006. Group 1B phospholipase A_2-mediated lysophospholipid absorption directly contributes to postprandial hyperglycemia. *Diabetes.* 55:935–941. http://dx.doi.org/10.2337/diabetes.55.04.06.db05-1286

Lowes, M.A., M. Suárez-Fariñas, and J.G. Krueger. 2014. Immunology of psoriasis. *Annu. Rev. Immunol.* 32:227–255. http://dx.doi.org/10.1146/annurev-immunol-032713-120225

MacPhee, M., K.P. Chepenik, R.A. Liddell, K.K. Nelson, L.D. Siracusa, and A.M. Buchberg. 1995. The secretory phospholipase A_2 gene is a candidate for the Mom1 locus, a major modifier of ApcMin-induced intestinal neoplasia. *Cell.* 81:957–966. http://dx.doi.org/10.1016/0092-8674(95)90015-2

Man, M.Q., T.K. Lin, J.L. Santiago, A. Celli, L. Zhong, Z.M. Huang, T. Roelandt, M. Hupe, J.P. Sundberg, K.A. Silva, et al. 2014. Basis for enhanced barrier function of pigmented skin. *J. Invest. Dermatol.* 134:2399–2407. http://dx.doi.org/10.1038/jid.2014.187

Mao-Qiang, M., M. Jain, K.R. Feingold, and P.M. Elias. 1996. Secretory phospholipase A_2 activity is required for permeability barrier homeostasis. *J. Invest. Dermatol.* 106:57–63. http://dx.doi.org/10.1111/1523-1747.ep12327246

Marichal, T., M. Tsai, and S.J. Galli. 2013. Mast cells: potential positive and negative roles in tumor biology. *Cancer Immunol Res.* 1:269–279. http://dx.doi.org/10.1158/2326-6066.CIR-13-0119

Miki, Y., K. Yamamoto, Y. Taketomi, H. Sato, K. Shimo, T. Kobayashi, Y. Ishikawa, T. Ishii, H. Nakanishi, K. Ikeda, et al. 2013. Lymphoid tissue phospholipase A_2 group IID resolves contact hypersensitivity by driving antiinflammatory lipid mediators. *J. Exp. Med.* 210:1217–1234.

Mulherkar, R., B.M. Kirtane, A. Ramchandani, N.P. Mansukhani, S. Kannan, and K.N. Naresh. 2003. Expression of enhancing factor/phospholipase A_2 in skin results in abnormal epidermis and increased sensitivity to chemical carcinogenesis. *Oncogene.* 22:1936–1944. http://dx.doi.org/10.1038/sj.onc.1206229

Murakami, M., Y. Taketomi, Y. Miki, H. Sato, T. Hirabayashi, and K. Yamamoto. 2011. Recent progress in phospholipase A_2 research: from cells to animals to humans. *Prog. Lipid Res.* 50:152–192. http://dx.doi.org/10.1016/j.plipres.2010.12.001

Murakami, M., H. Sato, Y. Miki, K. Yamamoto, and Y. Taketomi. 2015. A new era of secreted phospholipase A_2. *J. Lipid Res.* 56:1248–1261. http://dx.doi.org/10.1194/jlr.R058123

Nagamachi, M., D. Sakata, K. Kabashima, T. Furuyashiki, T. Murata, E. Segi-Nishida, K. Soontrapa, T. Matsuoka, Y. Miyachi, and S. Narumiya. 2007. Facilitation of Th1-mediated immune response by prostaglandin E receptor EP1. *J. Exp. Med.* 204:2865–2874. http://dx.doi.org/10.1084/jem.20070773

Oslund, R.C., N. Cermak, and M.H. Gelb. 2008. Highly specific and broadly potent inhibitors of mammalian secreted phospholipases A_2. *J. Med. Chem.* 51:4708–4714. http://dx.doi.org/10.1021/jm800422v

Pernet, E., L. Guillemot, P.R. Burgel, C. Martin, G. Lambeau, I. Sermet-Gaudelus, D. Sands, D. Leduc, P.C. Morand, L. Jeammet, et al. 2014. Pseudomonas aeruginosa eradicates Staphylococcus aureus by manipulating the host immunity. *Nat. Commun.* 5:5105. http://dx.doi.org/10.1038/ncomms6105

Sato, H., Y. Taketomi, Y. Isogai, Y. Miki, K. Yamamoto, S. Masuda, T. Hosono, S. Arata, Y. Ishikawa, T. Ishii, et al. 2010. Group III secreted phospholipase A_2 regulates epididymal sperm maturation and fertility in mice. *J. Clin. Invest.* 120:1400–1414. http://dx.doi.org/10.1172/JCI40493

Sato, H., Y. Taketomi, A. Ushida, Y. Isogai, T. Kojima, T. Hirabayashi, Y. Miki, K. Yamamoto, Y. Nishito, T. Kobayashi, et al. 2014. The adipocyte-inducible secreted phospholipases PLA2G5 and PLA2G2E play distinct roles in obesity. *Cell Metab.* 20:119–132. http://dx.doi.org/10.1016/j.cmet.2014.05.002

Schonthaler, H.B., J. Guinea-Viniegra, S.K. Wculek, I. Ruppen, P. Ximénez-Embún, A. Guío-Carrión, R. Navarro, N. Hogg, K. Ashman, and E.F. Wagner. 2013. S100A8-S100A9 protein complex mediates psoriasis by regulating the expression of complement factor C3. *Immunity.* 39:1171–1181. http://dx.doi.org/10.1016/j.immuni.2013.11.011

Serhan, C.N. 2014. Pro-resolving lipid mediators are leads for resolution physiology. *Nature.* 510:92–101. http://dx.doi.org/10.1038/nature13479

Serhan, C.N., C.B. Clish, J. Brannon, S.P. Colgan, N. Chiang, and K. Gronert. 2000. Novel functional sets of lipid-derived mediators with antiinflammatory actions generated from omega-3 fatty acids via cyclooxygenase 2-nonsteroidal antiinflammatory drugs and transcellular processing. *J. Exp. Med.* 192:1197–1204. http://dx.doi.org/10.1084/jem.192.8.1197

Serhan, C.N., K. Gotlinger, S. Hong, Y. Lu, J. Siegelman, T. Baer, R. Yang, S.P. Colgan, and N.A. Petasis. 2006. Anti-inflammatory actions of neuroprotectin D1/protectin D1 and its natural stereoisomers: assignments of dihydroxy-containing docosatrienes. *J. Immunol.* 176:1848–1859. http://dx.doi.org/10.4049/jimmunol.176.3.1848

Serhan, C.N., J. Dalli, R.A. Colas, J.W. Winkler, and N. Chiang. 2015. Protectins and maresins: New pro-resolving families of mediators in acute inflammation and resolution bioactive metabolome. *Biochim. Biophys. Acta.* 1851:397–413. http://dx.doi.org/10.1016/j.bbalip.2014.08.006

Singer, A.G., F. Ghomashchi, C. Le Calvez, J. Bollinger, S. Bezzine, M. Rouault, M. Sadilek, E. Nguyen, M. Lazdunski, G. Lambeau, and M.H. Gelb. 2002. Interfacial kinetic and binding properties of the complete set of human and mouse groups I, II, V, X, and XII secreted phospholipases A_2. *J. Biol. Chem.* 277:48535–48549. http://dx.doi.org/10.1074/jbc.M205855200

Smith, S.J., S. Cases, D.R. Jensen, H.C. Chen, E. Sande, B. Tow, D.A. Sanan, J. Raber, R.H. Eckel, and R.V. Farese Jr. 2000. Obesity resistance and multiple mechanisms of triglyceride synthesis in mice lacking Dgat. *Nat. Genet.* 25:87–90. http://dx.doi.org/10.1038/75651

Taketomi, Y., N. Ueno, T. Kojima, H. Sato, R. Murase, K. Yamamoto, S. Tanaka, M. Sakanaka, M. Nakamura, Y. Nishito, et al. 2013. Mast cell maturation is driven via a group III phospholipase A_2-prostaglandin D_2-DP1 receptor paracrine axis. *Nat. Immunol.* 14:554–563. http://dx.doi.org/10.1038/ni.2586

Tortola, L., E. Rosenwald, B. Abel, H. Blumberg, M. Schäfer, A.J. Coyle, J.C. Renauld, S. Werner, J. Kisielow, and M. Kopf. 2012. Psoriasiform dermatitis is driven by IL-36-mediated DC-keratinocyte crosstalk. *J. Clin. Invest.* 122:3965–3976. http://dx.doi.org/10.1172/JCI63451

Tu, C.L., D.A. Crumrine, M.Q. Man, W. Chang, H. Elalieh, M. You, P.M. Elias, and D.D. Bikle. 2012. Ablation of the calcium-sensing receptor in keratinocytes impairs epidermal differentiation and barrier function. *J. Invest. Dermatol.* 132:2350–2359. http://dx.doi.org/10.1038/jid.2012.159

Valentin, E., F. Ghomashchi, M.H. Gelb, M. Lazdunski, and G. Lambeau. 1999. On the diversity of secreted phospholipases A_2. Cloning, tissue distribution, and functional expression of two novel mouse group II enzymes. *J. Biol. Chem.* 274:31195–31202. http://dx.doi.org/10.1074/jbc.274.44.31195

Vasireddy, V., Y. Uchida, N. Salem Jr., S.Y. Kim, M.N. Mandal, G.B. Reddy, R. Bodepudi, N.L. Alderson, J.C. Brown, H. Hama, et al. 2007. Loss of functional ELOVL4 depletes very long-chain fatty acids (> or =C28) and the unique omega-O-acylceramides in skin leading to neonatal death. *Hum. Mol. Genet.* 16:471–482. http://dx.doi.org/10.1093/hmg/ddl480

Yamamoto, K., Y. Isogai, H. Sato, Y. Taketomi, and M. Murakami. 2011a. Secreted phospholipase A_2, lipoprotein hydrolysis, and atherosclerosis: integration with lipidomics. *Anal. Bioanal. Chem.* 400:1829–1842. http://dx.doi.org/10.1007/s00216-011-4864-z

Yamamoto, K., Y. Taketomi, Y. Isogai, Y. Miki, H. Sato, S. Masuda, Y. Nishito, K. Morioka, Y. Ishimoto, N. Suzuki, et al. 2011b. Hair follicular expression and function of group X secreted phospholipase A_2 in mouse skin. *J. Biol. Chem.* 286:11616–11631. http://dx.doi.org/10.1074/jbc.M110.206714